# Design, Modeling, and Fabrication of a Flapping Wing Micro Air Vehicle

Undergraduate Honors Thesis

Presented in Partial Fulfillment of the Requirements for
Graduation with Distinction in Mechanical Engineering

by

Jeff Kohler

The Ohio State University

March 2013

Advisor: Haijun Su

# ABSTRACT

The purpose of this research is to design and fabricate a flapping wing micro air vehicle (MAV) using compliant mechanisms and shape deposition manufacturing (SDM). A compliant mechanism is a device that transfers motion, force, or energy and gains at least some of its mobility through the elastic deformation of flexible members. This allows for a reduction of parts and weight, low friction and maintenance, and high precision. Shape deposition manufacturing is a rapid prototyping technology for building up material layers to form complex-shaped, multi-material, embedded-component structures. It allows for lower-cost, near net shape fabrication. A preliminary design was created and analyzed using kinematic software to determine the mechanism's functionality and the overall structure's ability to maintain flight. The prototype was fabricated using shape deposition manufacturing, but was not functional due to an error in the design calculations. Changes were made to the design and a second prototype was fabricated. The second prototype is currently not functional due to a problem with the motor. Design iterations will continue to improve the design and once a functioning prototype is produced, the MAV will be tested to determine how much lift it can produce. Experiments will be conducted with different wing designs to find optimal lift performance. If successful, this could lead to a new approach used by designers around the world.

# ACKNOWLEDGEMENTS

I would like to thank my advisor, Dr. Haijun Su, for his continued support and guidance. He has willingly provided the resources necessary in completing this project and has dedicated his time to ensure my success. I would also like to acknowledge OSU for allowing me to use their facilities and resources.

I am also appreciative of the aid I have received from the other students in the Design, Innoviation, and Simulation Lab (DISL). John King has been very helpful in introducing us to the Shape Deposition Manufacturing process. He has provided helpful design advice and completed a large amount of the tasks associated with fabricating the prototype. Venkatasubramanian Venkiteswaran has also helped with the design process and analyzing the dynamic model of the MAV. Finally, Jon Cleary has provided guidance along the way and helped fabricate the second prototype.

I would like to recognize the head of the machine shop at Scott Lab, Chad Bivens, for writing the code necessary to machine the first prototype. He was very helpful and patient when working with me during the fabrication process. The first prototype would not have been created if it were not for his help.

# TABLE OF CONTENTS

# LIST OF FIGURES

# LIST OF TABLES

# CHAPTER 1: INTRODUCTION

## 1.1 Background

The micro air vehicle (MAV) program was created by the Defense Advanced Research Projects Agency (DARPA) in 1996 for developing small autonomous flying vehicles. MAVs were defined as aircrafts that were smaller than 15 cm in length, width, or height. Their intended uses include reconnaissance missions, chemical and biological detection, and surveillance in unstable areas. MAVs will give a soldier the ability to increase their situational awareness without the need to be put in harm's way. With the capability to operate in constrained environments, MAVs will possess the ability to complete missions indoors as well [1].

There are three categories of MAVs that exhibit active propulsion: fixed wing, rotary wing, and flapping wing. Fixed wing are the most developed and easiest to design because of the capability of scaling down larger aircraft. This category requires high speeds to maintain flight and therefore is not suitable for hovering or low speed flight. They are more apt for long range, outdoor missions [2]. An example of a fixed wing MAV is the Black Widow, developed by AeroVironment in 2001 (Figure 1 [3]).


Figure 1: AeroVironment's Black Widow

The rotary wing category is comprised of smaller scale helicopters. They have the ability to achieve high speeds, hover, and execute vertical takeoff and landing. This makes them ideal for short range, indoor missions. However, large power consumption and significant noise production are the challenges this category faces [2]. An example of a rotary wing MAV is the Shrediquette, developed by a researcher in Germany in 2010 (Figure 2 [4]).


Figure 2: William Thielicke's Shrediquette

Both the fixed and rotary wing technologies are well studied and documented, but have problems with unsteady effects due to a reduction of the Reynolds number when scaling down to the micro size. An alternative that is increasing in popularity is the flapping wing MAV. This category mimics the motion that is used by birds and insects as seen in nature. Numerous studies are being completed to determine how to integrate lift and thrust production with stability and control of the vehicle. The advantages of this category are the increased efficiency of lift production and the ability to generate numerous flight maneuvers [2]. An example of a successful flapping wing MAV is the Nano Hummingbird from AeroVironment in 2012 (Figure 3 [5]).

Figure 3: AeroVironment's Nano Hummingbird

Researchers have increased the study of bird and insect flight to improve the design of MAVs. Many studies have been conducted to map the path of wings during takeoff, cruise, hovering, and landing as well as the air flow over the wings to see the advantages of the angle of attack. The muscular motions of birds and insects have also been studied to find an efficient mechanism to provide a flapping motion [6]. MAVs, however, face many challenges when attempting to mimic bird and insect flight. Birds and insects have the freedom to adjust the angle of attack, flapping frequency, and pitch freely and instantaneously. In MAVs, every adjustment of angle of attack, flapping frequency, and pitch must be controlled and executed by a driving mechanism. Every control not only adds weight, but consumes power, and so decreasing the flight time capability of the vehicle.

This research will attempt to use unexplored techniques in the field of flapping wing MAVs in order to decrease the weight of the vehicle and increase the efficiency. The two techniques are the elimination of rigid joints by using compliant mechanisms and the use of shape deposition manufacturing to create the structure. The advantages of each technique will be further explored below.

## 1.2 Compliant Mechanisms

A mechanism is a mechanical device that is used to transfer input motion into a desired output motion. Rigid body mechanisms typically consist of rigid links connected at movable joints, as shown in Figure 4(a). Comparatively, compliant mechanisms consist of flexible members or joints and receive at least some of their mobility from the deflection of the flexible members, as shown in Figure 4(b) [7].

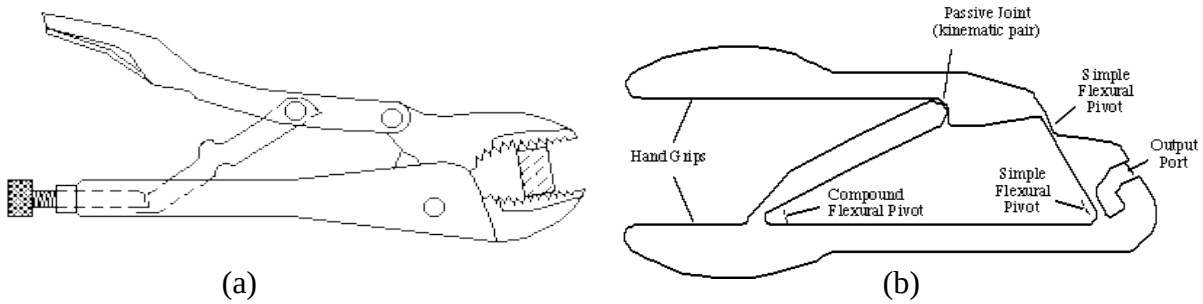


Figure 4: (a) Rigid Body Gripper Mechanism vs. (b) Compliant Gripper Mechanism

There are numerous advantages that compliant mechanisms present. From the figure above, one can see there is a large reduction in the number of parts required to accomplish a specific task. In most cases, this will reduce the manufacturing and assembly time and cost. This reduction of parts can also result in a much lighter mechanism. The removal of rigid joints eliminates the friction that would normally be present in the mechanism. One may also factor the stored energy of a deflected member into the compliant mechanism design and use it to complete a specific action. Another advantage is the ease in which compliant mechanisms are miniaturized. It is simpler to create a single small part as opposed to an assembly of miniature parts [7].

The analysis of complaint mechanisms is completed using pseudo rigid body models (PRBM). A single flexible member is replaced with two rigid links, a pivot point, and a torsional spring, as shown in Figure 5. Knowing the mechanical properties of the link, one can

approximate the final position when a force is applied. This allows well know rigid body analysis models to be used in the analysis of compliant mechanisms. This principle can be applied to larger and more complex compliant mechanisms and be used in the analysis of input force requirements and output motion prediction [7].

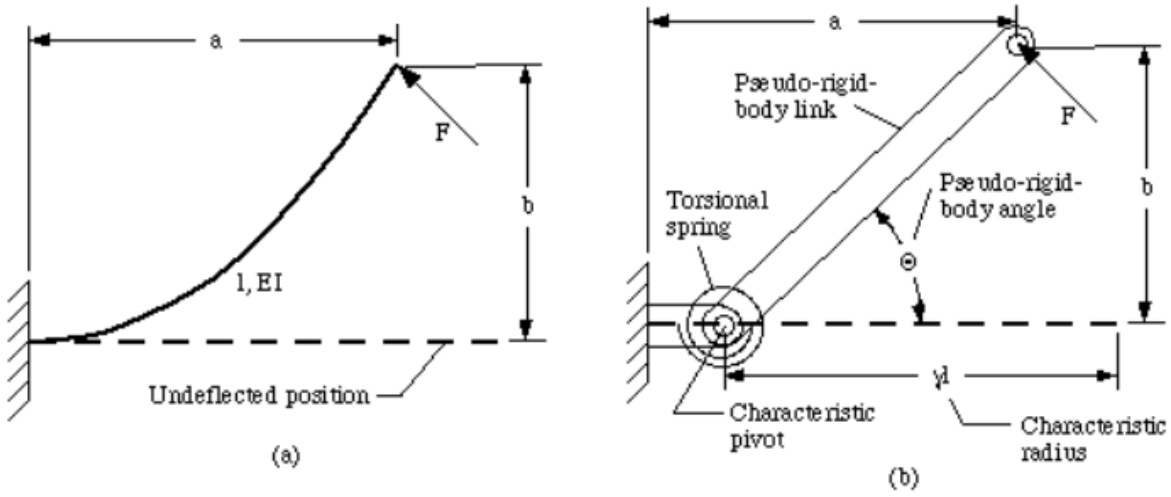


Figure 5: (a) Compliant Member (b) PRBM of Compliant Member

### 1.3 Shape Deposition Manufacturing

Shape Deposition Manufacturing (SDM) is a rapid prototyping technology for building up material layers to form complex-shaped, multi-material, embedded-component structures. The method of SDM is to deposit support material and part segments layer by layer to form a complete part. The support material is then removed to leave the final part, as shown in Figure 6 [8]. This process also provides the ability to use multiple materials and embed components in the separate layers [9]. Therefore with relatively simple machining practices, a complex, multi-material structure can be formed with embedded components as shown in Figure 7 [8].

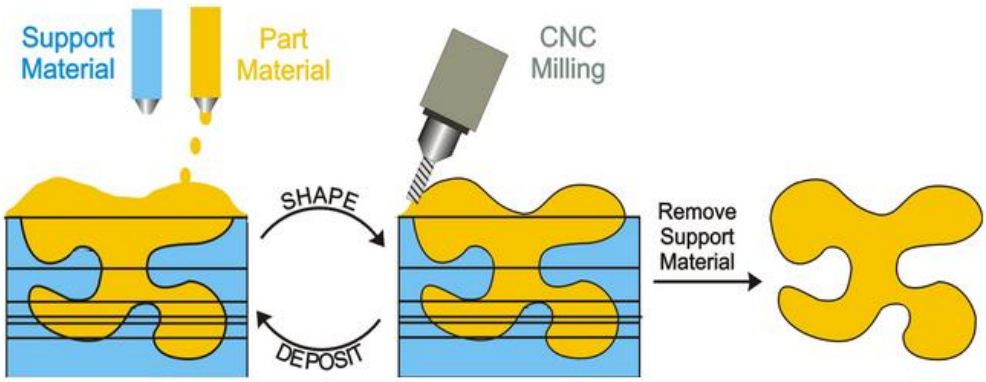


Figure 6: Shape Deposition Manufacturing Process

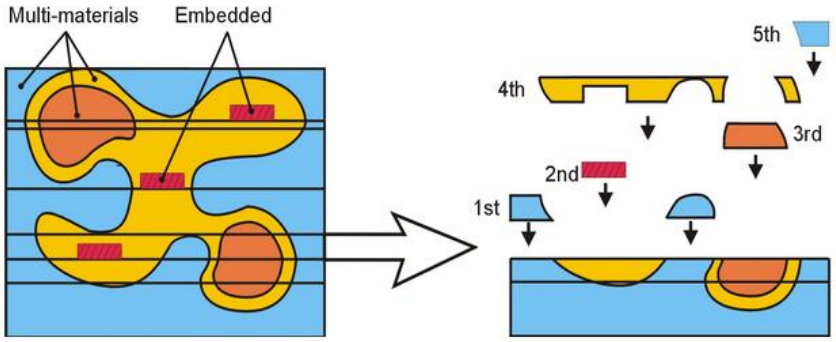


Figure 7: SDM with Multiple Materials and Embedded Components

SDM pairs well with compliant mechanisms because of the ability to create a single complex structure. Take for example, the complaint gripper mechanism in Figure 4. The shape of this structure could first be machined into the support material. Then the desired part material would be poured into this mold and allowed to cure. Finally the part is extracted and ready for use. This greatly simplifies the manufacturing process when compared to the equivalent rigid body mechanism, of which each individual part has to be manufactured and then assembled.

### 1.4 Overview of Thesis

The thesis has six chapters. Chapter 2 discusses the initial design process of the MAV. It will overview the initial concepts, preliminary kinematic and dynamic analysis, and explains the reasoning for pursuing the final prototype design. Chapter 3 will discuss some of the design

modifications encountered on the way to construction and explain how the final design developed. Chapter 4 will overview the manufacturing of the prototype, focusing on the shape deposition manufacturing process. Chapter 5 discusses the testing and results of the prototype. Chapter 6 will discuss changes from the first prototype to the second prototype. Finally, Chapter 7 will conclude the thesis and recommend further actions.

# CHAPTER 2: FIRST DESIGN ITERATION

## 2.1 Ornithopter vs. Entomopter Design

One of the major design decisions that needed to be made early in the design process was whether to pursue a design that fly's forward, similar to birds, or hovers, similar to insects. Ornithopters are vehicles that mimic the flapping kinematics of birds. They use an up and down flapping motion with small variance in the attack angle, as shown in Figure 8. These primarily require a forward velocity to produce enough lift to remain in flight. Entomopters are vehicles that mimic the flapping kinematics of insects. These use large variances in wing angle and typically have a pitch reversal, which flips the direction of the leading edge of the wing, as shown in Figure 9. They use high angles of attack and wing tip vortices to generate enough lift to sustain flight [10].

Figure 8: Wing Path of an Ornithopter

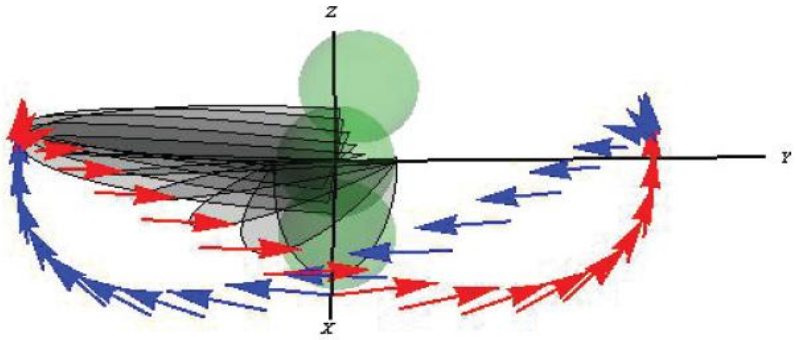


Figure 9: Wing Path of an Entomopter

The advantage of creating a design that hovers is that it is easier to test. A long hallway is required to test a flapping wing MAV that requires forward velocity to maintain flight, while a hovering aircraft can be tested in a confined space. The challenge of designing a hovering flapping wing MAV is the wings must change their angle of attack when flapping from one direction to the other so that they are always generating positive lift. As seen in Figure 9, the leading edge must reverse directions between the forward stroke and backward stroke. This requires either active or passive control of the angle of attack of the wing. This is not required for the ornithopter flight, as the wings must only perform an up and down motion at a constant angle of attack.

The choice was made to pursue a design that hovers. The main factor was the ease of testing. It will be much easier to determine the amount of lift produced by the MAV when it is only generating an upward motion. For forward flight, only a qualitative analysis can be performed to determine if the vehicle does indeed produce enough lift to sustain flight, and even then it will vary based on the initial forward velocity given. The design of the wing will be more complex as now it will need to be controlled. Previous solutions for wing control will be studied in order to determine an appropriate method.

## 2.2 Linear vs. Rotary Actuator

Another major design decision that occurred early in the design process was whether to use a linear or rotary actuator. Bolsman [11] has studied the different actuators that are available for MAV applications. Among the ones with the most potential are piezoelectric linear actuators and geared down rotational DC motors.

Piezoelectric actuators are ideal because they provide a linear motion which is ultimately required to create a flapping motion. They have a high efficiency of power conversion and are easy to precisely control. The main deficiencies are that they require a very high voltage to operate, approximately 100-200 volts, and they produce very little displacement, on the order of millimeters.

Rotational DC motors are another valid option, but the rotational motion has to be converted to a linear motion to create a flapping mechanism. They too have a high efficiency and control over rotational speed. DC motors, however, operate at a much lower voltage, approximately 3-6 volts. These motors usually produce very high rpm's; therefore they need to be geared down to produce a flapping frequency that is more reasonable.

The decision was made to choose the geared down rotational DC motor because of the lower voltage required. This gives the ability of the design to be autonomous, as a light weight battery can be attached to the structure of the MAV to provide the required voltage. With a piezoelectric actuator, an external power source connected to the ground is used to provide the required voltage.

## 2.3 Converting Rotational Motion into Linear Motion

A common approach for converting an input of rotational motion to an output of linear motion is to use a crank-slider mechanism, as pictured in Figure 10. The DC motor is fixed and

will rotate the crank, which is connected to a coupler, which drives the slider in a translational motion. The slider is usually contained in a groove to limit its motion to along only one axis. The friction created by the slider rubbing against the constraining walls is a concern for this design, and is being pursued as an area to use a compliant mechanism.

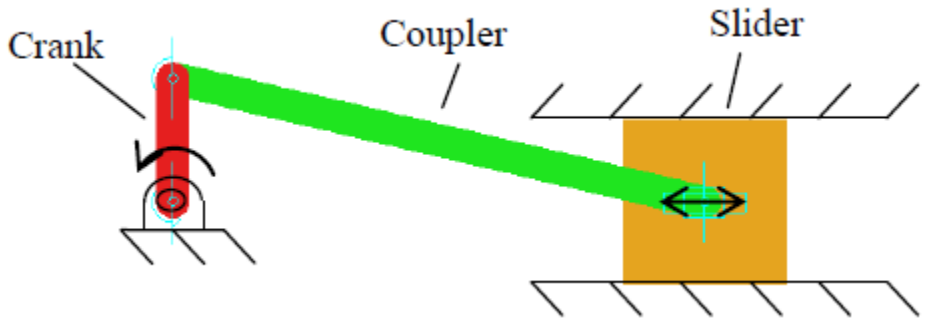


Figure 10: Crank-Slider Mechanism

A compliant mechanism can be introduced to this design at the slider. This mechanism is called a parallel guiding mechanism, shown in Figure 11. The mechanism is fixed on the right hand side, with a rigid body on the left hand side. Two flexible links connect the fixed side to the rigid body. These links are made flexible by simply decreasing their thickness. This type of mechanism will exhibit high stiffness in the x-direction and low stiffness in the y-direction. This is because a force applied solely in the x-direction will attempt to make the links buckle, which typically requires a high force. This mechanism can replace a slider because it will keep the slider centered along the desired path, the y-axis, due to the high stiffness in the x-direction.

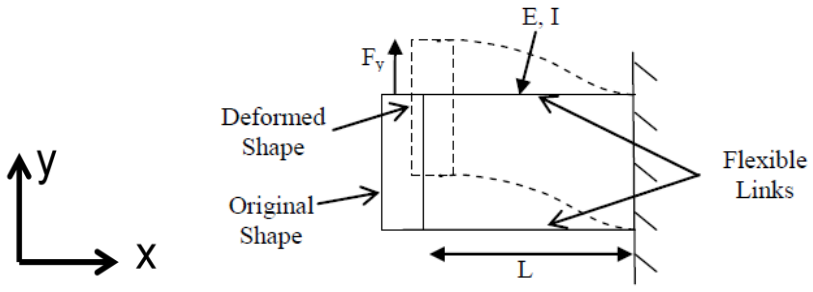


Figure 11: Parallel Guiding Mechanism

Simply by knowing the force applied ($F_y$), the Young's Modulus of the material (E), and the moment of inertia (I) and length (L) of the flexible links, one can predict the location of the deformed shape using pseudo rigid body models. Several of these mechanisms can be combined to create a mechanism that has a larger displacement and an increased stiffness in the x-direction. This will be referred to as the combined parallel guiding mechanism, and is pictured in Figure 12. This mechanism is made up of four of the parallel guiding mechanisms. The central back square in the figure is fixed, while the central forward square has a vertical force applied. The resulting deformed mechanism is shown in Figure 13. Again, this mechanism is used to increase the resulting displacement and increase the stiffness in the off-axis direction.

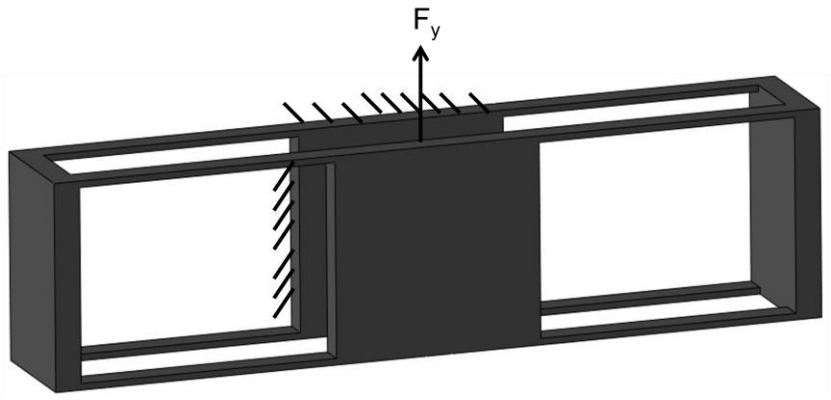


Figure 12: Combined Parallel Guiding Mechanism

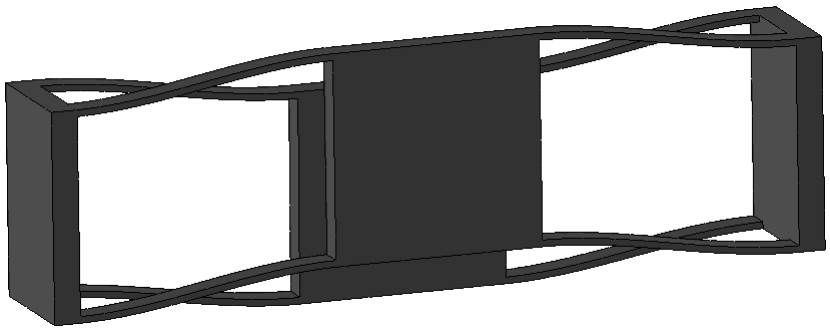

Figure 13: Displaced Model of Combined Parallel Guiding Mechanism

## 2.4 Pseudo Rigid Body Analysis

The combined parallel guiding mechanism can be analyzed using approaches found in [7]. First, the parallel guiding mechanism will be examined by itself. The flexible links are in a fixed-guided arrangement, so they were replaced with three rigid links and two torsional springs, as shown in Figure 14.

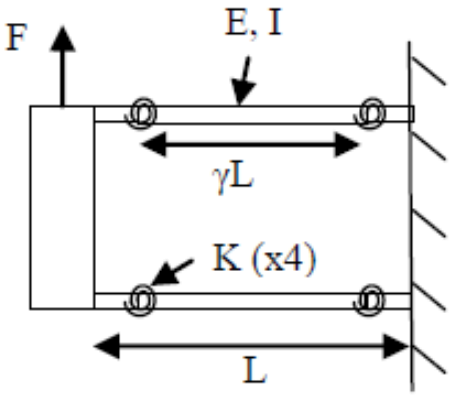


Figure 14: PRBM of Parallel Guiding Mechanism

The torsional stiffness of each spring, K, was found using Equation 1, where γ and $K_\theta$ are constants.

$$K = \frac{2\gamma K_\theta EI}{L} \tag{1}$$

Where Δθ is the change in the angle of the middle rigid link, Equations 2 and 3 give the vertical force required, $F_y$, and the change in vertical height, Δy, respectively.

$$F_y = \frac{4K\Delta\theta}{\gamma L cos(\Delta\theta)} \tag{2}$$

$$\Delta y = \gamma L \sin(\Delta\theta) \tag{3}$$

If Δθ is small, then cos(Δθ) = 1 and sin(Δθ) = Δθ. The vertical stiffness of each parallel guiding mechanism, $K_y$, is given by Equation 4.

$$K_y = \frac{F_y}{\Delta y} = \frac{4K}{(\gamma L)^2} \tag{4}$$

The spring model of the combined parallel guiding mechanism is represented as shown in Figure 15. It is represented by a pair of parallel springs, each with two springs in series.

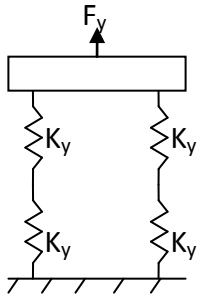


Figure 15: Spring Model of Combined Parallel Guiding Mechanism

The overall vertical stiffness of the mechanism, $K_m$, is given by Equation 5.

$$K_m = 2\left(\frac{K_y}{2}\right) = K_y = \frac{4K}{(\gamma L)^2} \tag{5}$$

Knowing the PRBM results would vary from actual results at larger displacements, Equation 5 was used to approach a desired stiffness. The combined parallel guiding mechanism was then modeled in the SolidWorks Finite Element Analysis (FEA) package to the find the vertical stiffness of the mechanism and then compared to the PRBM results.

## 2.5 Designing the Compliant Mechanism

A mechanism was desired that provided enough stiffness in the off-axis direction, but did not require a large force to be displaced. The larger the force required, the larger the torque that must be produced by the motor. Upon searching for lightweight geared down DC motors, the average torque was found to be around 10 N-mm. It was desired to use no more than 10% of this torque on displacing the mechanism, as a significant amount will be required to produce lift. The crank size determines the maximum amount the mechanism will be displaced, based on when the crank and coupler are aligned in Figure 10. Enough displacement needs to occur in order to translate this into a large flapping angle, but the larger the crank size, the more torque required.

A crank size of 5 mm was determined to be sufficient in preliminary design sketches to generate a flapping angle of 100°. Using the model shown in Figure 16, the force at the end of the crank opposite from the motor will be the torque multiplied by the length of the crank. The coupler is a two force member, so the same force on the crank will be transmitted to the slider. Using the size of the crank as the displacement of the slider, and 10% of the average torque of the motors, one can find a desired stiffness of the mechanism. Using this approach, the desired stiffness is 40 N/m. This will be used as a goal for the initial design.

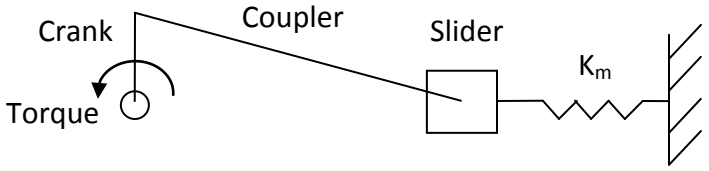


Figure 16: Crank-Slider Stiffness Model

A lightweight material with good strength to elasticity qualities is polypropylene. The first design was created using the properties of this material (E = .896 GPa) [7]. Several iterations were performed to create a combined parallel guiding mechanism with a stiffness near 40 N/m. Without making the mechanism too wide and too thin, the dimensions shown in Figure 17 were chosen as a suitable first design. The depth of each parallel guiding mechanism into the page is 2 mm. If the sketch were an isotropic view, it would resemble Figure 12.

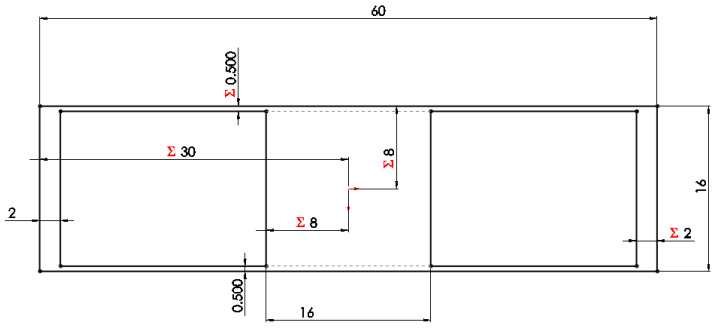


Figure 17: Dimensions of Combined Parallel Guiding Mechanism

The stiffness was calculated using the PRBM and SolidWorks FEA software. The result of each is shown in Table 1. As mentioned earlier, the stiffness of the PRBM is only accurate for small deflections. The mechanism needs to deflect 5 mm, which is too large for the assumptions of the PRBM. The setup of the analysis and the results are shown in Figures 18 and 19, respectively. From the FEA analysis, the mechanism requires .261 N to deflect 5 mm. The PRBM provided a quick and easy approximation that was later refined in the FEA analysis.

Table 1: Stiffness of Mechanism

| Method | PRBM | FEA | % Difference |
|---|---|---|---|
| Stiffness, $K_m$ (N/m) | 58.8 | 52.2 | 11.2 % |

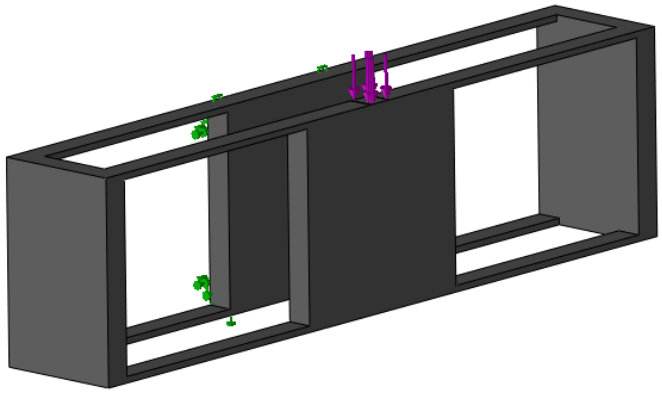

Figure 18: Setup of SolidWorks FEA Analysis

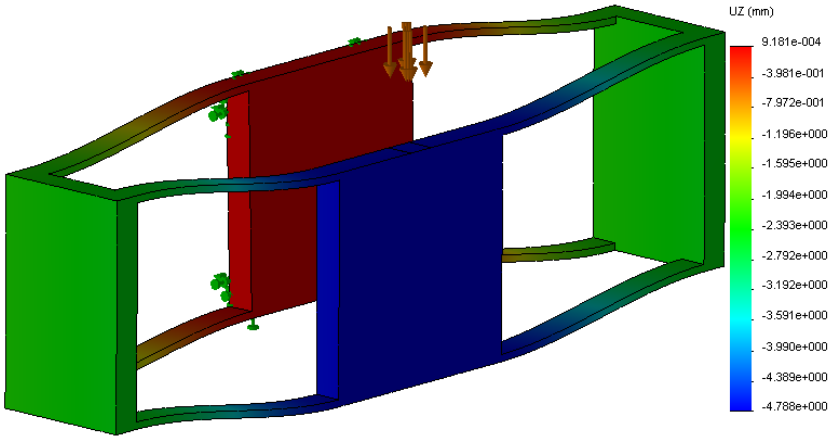


Figure 19: FEA Analysis Deflection Results

## 2.6 Motor and Battery Selection

Knowing the approximate torque that would be required, about 10 N-mm, a low-cost, lightweight geared down motor was selected from a supplier. The motor selected was the GM15A gear motor from Solarbotics©, shown in Figure 20. The specifications of the motor given by the manufacturer are shown in Table 2. The motor weighs 1.3 grams and comes with a D-profile shaft, which makes connecting it to the crank simple [12].

Figure 20: Solarbotics© GM15A Motor

Table 2: Specifications for GM15A Motor

| Voltage (V) | Unloaded RPM | Unloaded Current (mA) | Stall Current (mA) | Stall Torque (Nmm) |
|---|---|---|---|---|
| 3 | 920 | 100 | 210 | 3.46 |
| 6 | 1550 | 200 | 350 | 6.80 |

The type of battery that was selected to pursue was the rechargeable Lithium-Polymer (LiPo) battery. These exhibit very large energy density and are common among other MAVs [13]. The standard voltage of a single LiPo cell is given as 3.7 V. They can range, however, from 3 to 4.2 V, during safe operation between full discharge and full charge, respectively. When selecting a battery, a couple of important specifications are the capacity, in mAh, and discharge rate, usually a multiple of capacity [14]. Assuming our motor is drawing 300 mA of current, a battery with a capacity of 30 mAh and a discharge rate of 10C would be suitable for this application. The duration of the flight would be the capacity divided by the current, which gives approximately six minutes.

One will notice from Table 2 that to reach the approximate torque of 10 N-mm, a voltage of greater than 6 volts would need to be applied. When batteries are connected in series, their

voltages add and the capacity remains constant. Therefore, a LiPo battery pack can be created with two batteries in series that delivers from 6 to 8.4 V, ranging from full discharge and full charge states, respectively. The stall torque and no load rpm will both increase with the larger voltage applied, as seen from the increase from 3 to 6 V. Two batteries would increase the weight of the structure significantly so it was important to find light weight, low capacity batteries that would be suitable for short flight times as opposed to heavier, high capacity batteries. The batteries that were selected were the Full River© 30 mAh, 10C from BSD Micro RC, pictured in Figure 21. A single cell weighs 1.1 grams [15].

Figure 21: Full River© 30 mAh 10C LiPo Battery

## 2.7 Designing the Structure

Once the combined parallel guiding mechanism was developed, a MAV structure was built that used it as a slider in a crank-slider mechanism. To begin, a sketch was made in SolidWorks to test functionality. The sketch was used to find the limits of the flapping angle and check for interferences. The limits of the flapping angle are ± 50°. The final sketch and its dimensions, in millimeters, is shown in Figure 22.

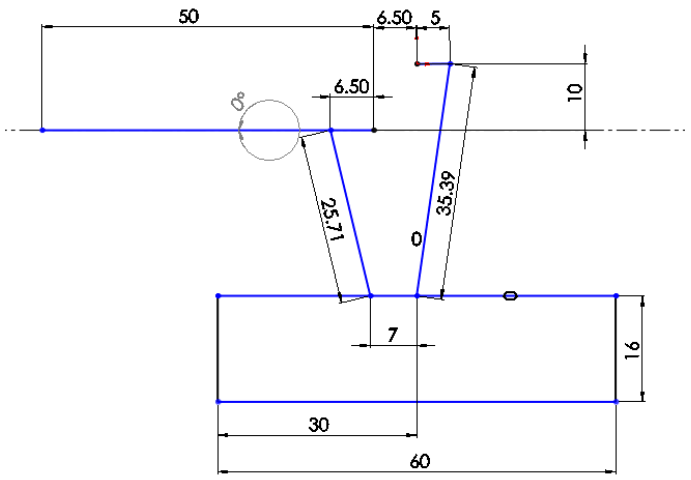


Figure 22: Kinematic Sketch of MAV Structure

Next, a simple to manufacture structure was developed. Using SolidWorks and the dimensions from Figure 22, the design was created as shown as a front view in Figure 23 and an isometric view in Figure 24.

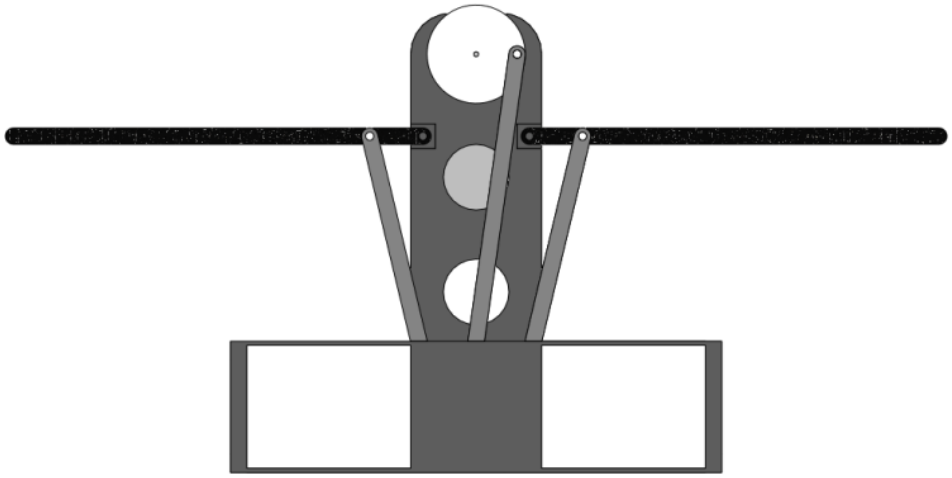

Figure 23: Front View of MAV Structure

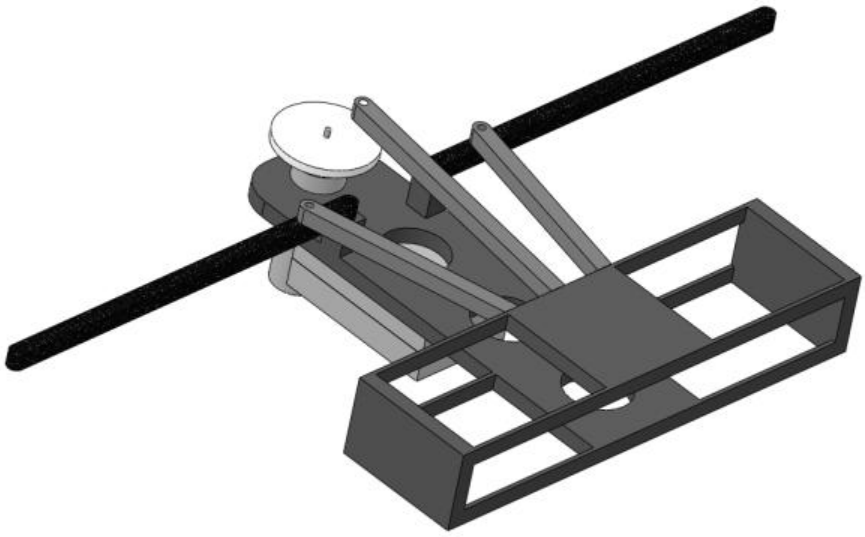

Figure 24: Isometric View of MAV Structure

The assembly was created with the idea that shape deposition manufacturing (SDM) would be used. The assembly could be poured in three simple layers. The layers are depicted in Figures 25-27.

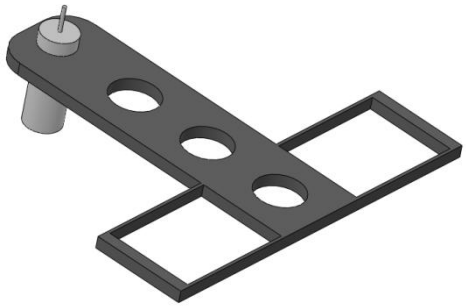

Figure 25: First Layer of SDM

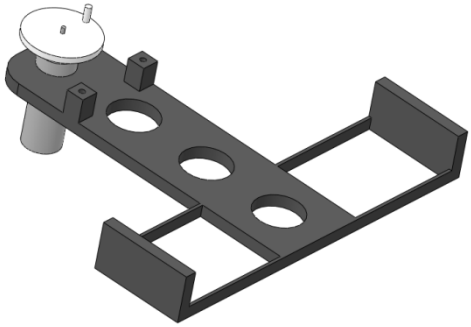

Figure 26: Second Layer of SDM

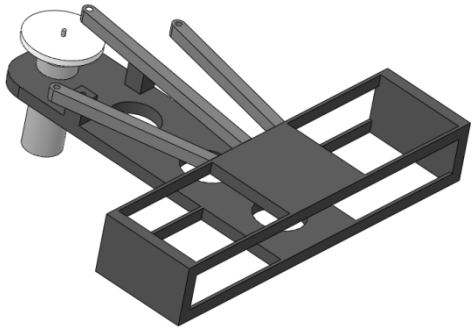

Figure 27: Third Layer of SDM

A urethane with similar properties to polypropylene will be used for all three layers. In Figure 25, the first layer will be poured with the motor embedded. The second layer, shown in Figure 26, is used to connect the first to the third, and contains the wing arm pivot points and the crank. The third layer, in Figure 27, contains the coupler and the wing activators, which will be poured with pivots embedded, such that they can achieve the small angle deflections where they meet the slider. The batteries will be attached to the bottom side of the structure using a non-permanent attachment method. The wing supports will be carbon fiber rods and will be attached after the SDM process. The final structure after assembly is complete will appear as seen in Figure 24. The final weight of the structure is 8 g, and is broken down as shown in Table 3.

Table 3: Weight Distribution of MAV

| Part | Weight | % of Weight |
|---|---|---|
| SDM Structure | 2.8 g | 35% |
| Crank | .16 g | 2% |
| Solarbotics GM15 Motor | 1.3 g | 16.25% |
| Wing Supports | .74 g | 9.25% |
| Full River Batteries | 2.2 g | 27.5% |
| Wings | .8 g | 10% |

## 2.8 Analyzing the MAV

After determining the dimensions of the MAV, the structure was modeled using kinematic software, MSC Adams-View, to determine some numerical parameters, such as lift produced and torque required. The equations used in Adams to model the torque of the motor

and the lift produced by the wings are presented below. They use real time data within Adams to continuously calculate their values. Equation 6 was used to model the motor torque, $\tau$, using values taken from the motor specification sheet, shown in Table 2: $\tau_s$, the stall torque, and $\omega_o$, the no load speed; and the real time variable $\omega_c$, the crank's rotational velocity. Equation 7 was used to model the drag force on the wing, $F_D$, using several constants: $\rho_a$, the density of air, $C_D$, the drag coefficient, $\alpha$, the angle of attack, L, the depth of the wing, and R, the wing span of one wing; and the real time variable $\omega_w$, the wing's rotational velocity [16]. The drag force is equivalent to the lift produced by the wing, $F_L$, at an angle of attack of 45°.

$$\tau = \tau_s - \frac{\tau_s}{\omega_o}\omega_c \tag{6}$$

$$F_D = \pm\frac{1}{6}\rho_a C_D \cos(\alpha)\, LR^3\omega_w \tag{7}$$

The simulation was setup as shown in Figure 28. A spring with the same stiffness as the combined parallel guiding mechanism was applied instead of using flexible bodies to greatly decrease the simulation time.

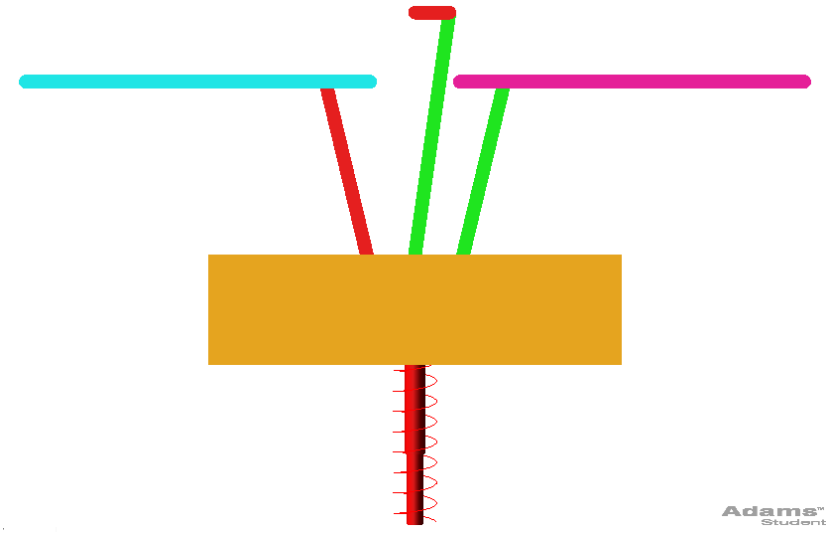


Figure 28: Adams Simulation Setup

Equation 6 was used to apply a continuously varying torque on the crank. The motor specifications were taken from the manufacturer's website, assuming a 6 V power source [12]. The equation also used an "if" statement to prevent the torque from being negative, as it is a motor, not a generator. The torque plot is shown in red in Figure 29.

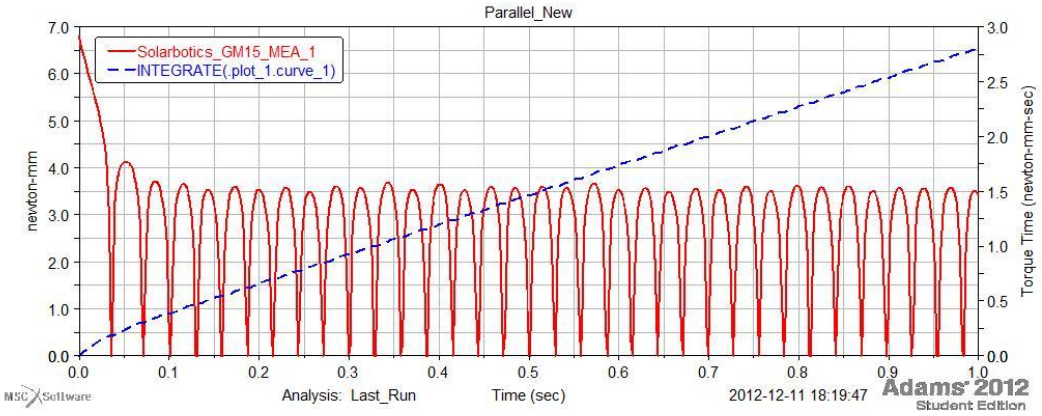


Figure 29: Motor Torque Plot

To find the average torque, the integral of the curve, shown in blue in Figure 29, was taken over a period of one second. The average torque required was 2.75 N-mm. The maximum torque required was 3.5 N-mm. The motor is capable of producing up to 7 N-mm at 6 V.

Equation 7 was used to apply a continuously varying drag force on the wing. The assumed wing size was similar to the size of the Nano Hummingbird wing, R = 100 mm and L = 30 mm [5]. The force always opposes the direction of motion. As previously mentioned, at the angle of attack used, 45°, the drag force is equivalent to the lift force. Therefore the force will be referred to as lift. The lift force plot for one wing is shown in red in Figure 30.

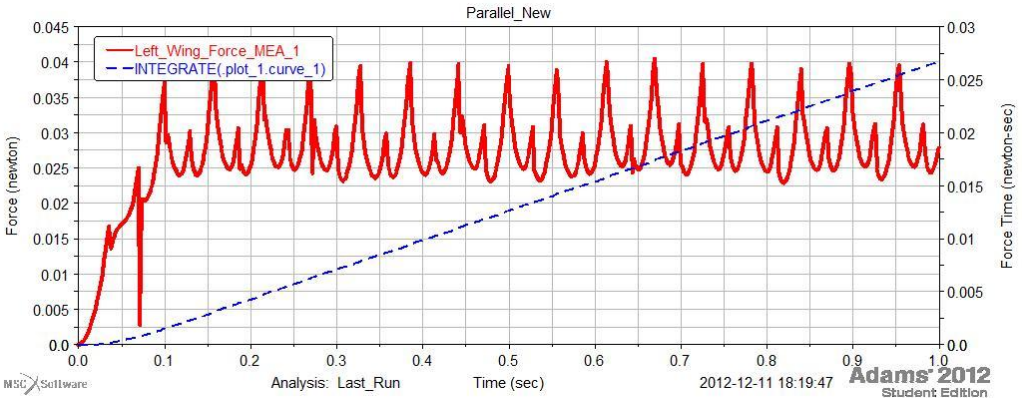


Figure 30: Lift Force Plot for One Wing

Just as for the torque, the integral was taken and the average lift produced by one wing was 0.0275 N. With two wings, this could support a load of 5.6 g. At 8 g, this design would not be able to produce enough lift to sustain flight. Weight reductions and wing size variations will be explored to increase the lift and decrease the weight. With the loads applied, a flapping frequency of 17 Hz was observed.

## 2.9 Conclusions of First Design

The MAV as it is currently designed is not capable of sustaining flight, as it is 2.4 g too heavy. Weight reductions need to be explored, especially in the SDM structure and the batteries, considering that they are the two heaviest components and easiest to modify. Modifications can also occur to the wing size. An increased wing area would result in increased lift production.

The current kinematic model assumes a 6 V power source. The current power source consists of two 3.7 V Li-Poly batteries connected in series. This will provide 7.4 V to the motor. If the motor can withstand 7.4 V without burning out, this will increase the torque produced and the speed of the motor. Increasing the flapping frequency of the MAV will result in more lift production. If the motor cannot withstand 7.4 V, a voltage regulator or resistor will need to be integrated into the circuit. This will allow the motor to function properly but decrease the efficiency of the MAV.

# CHAPTER 3: SECOND ITERATION DESIGN FOR PROTOTYPE

## 3.1 Design Approach for using SDM Materials

The SDM process, which is outlined in Chapter 4, requires creating a mold, pouring the material into the mold, allowing the material to cure, and finally extracting the parts. The initial concept was to find a material with properties similar to polypropylene to use for the whole structure. Upon further investigation, the concept of using two materials, one stiff and one flexible, became more attractive. Urethane plastic would be used as a stiff material where rigidness is desired. Urethane rubber would be used as a flexible material where elasticity is desired. This is more advantageous because the flexibility of the mechanism can be better controlled with small joints. Also, rubber has a much greater fatigue life compared to thin cross-sections of polypropylene.

Another concept that was further pursued was pouring two separate bodies and connecting them upon extraction. When viewing Figures 25-27, there are three layers that need to be created, with the use of sacrificial material to create a gap between the first and third layer. Without the availability of sacrificial material, the idea of creating the first and third layers as separate bodies and connecting them became ideal. It would greatly simplify the machining process.

## 3.2 Redesign of Compliant Mechanism for SDM Materials

The compliant mechanism had to be redesigned for the use of two different materials. The two materials selected were from Smooth-On©. The urethane plastic was TASK© 9 and the urethane rubber was VytaFlex© 60. The properties of each can be found here [17]. The design was adjusted to incorporate using two materials instead of one. Since rubber has a lower modulus of elasticity than polypropylene, the combined parallel guiding mechanism could be

sized down and remain at the same stiffness. Instead of long thin flexible beams like the original design (see Figure 11), the rubber will be short segments and treated as living hinges, see Figure 31. The analysis changes slightly, but only by the calculation of the stiffness for the torsional spring and the length of the middle rigid link. The PRBM is shown in Figure 32.

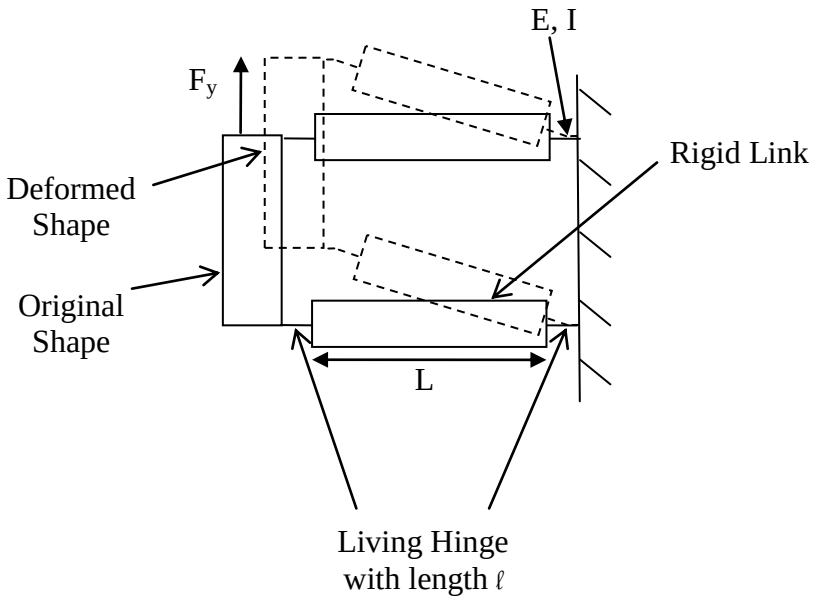


Figure 31: Parallel Guiding Mechanism with Living Hinges

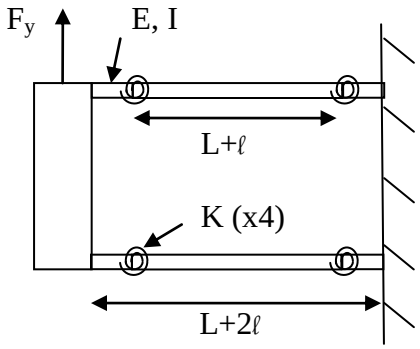


Figure 32: PRBM of Parallel Guiding Mechanism with Living Hinges

The equations for the analysis are similar to Equations 1 through 4. The torsional spring stiffness for each living hinge, K, was found using Equation 8. The vertical force and displacement are shown in Equations 9 and 10, respectively.

$$K = \frac{EI}{\ell} \tag{8}$$

$$F_y = \frac{4K\Delta\theta}{(L+\ell)cos(\Delta\theta)} \tag{9}$$

$$\Delta y = (L+\ell)\sin(\Delta\theta) \tag{10}$$

Using the same approximation as before, if $\Delta\theta$ is small, then $\cos(\Delta\theta) = 1$ and $\sin(\Delta\theta) = \Delta\theta$. The vertical stiffness of each parallel guiding mechanism, Ky, is given by Equation 11.

$$K_y = \frac{F_y}{\Delta y} = \frac{4K}{(L+\ell)^2} \tag{11}$$

Again the PRBM was used to approach the desired stiffness using different cross sections and lengths of segments.

### 3.3 Redesign of Structure

While determining the approximate stiffness of the mechanism, it was observed that the mechanism was much more flexible due to the rubber having a much smaller modulus of elasticity. To simplify the design, it was decided to only use the parallel guiding mechanism on the third layer. The first layer would just be solid and act as the ground for the third layer. The final mechanism as designed is shown in Figure 33. The bottom layer is shown in grey, and as mentioned is solid rigid material. The top layer is shown in transparent blue and green. The transparent blue is the rigid material and the green is the flexible joints. The two layers are connected using a raised boss on the bottom layer and a cut out in the top layer.

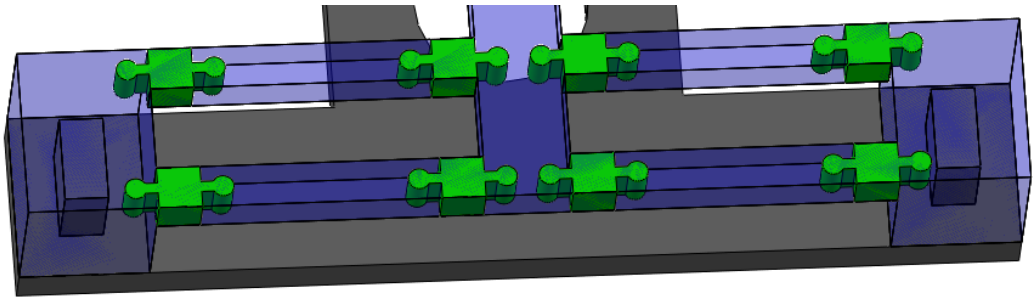

Figure 33: First Prototype Parallel Guiding Mechanism

The complex shape of the joints was to ensure the flexible material created a lasting bond with the rigid material. As our lab had not previously worked with the SDM process, the goal was to create a geometry that did not depend on the two surfaces bonding. Test links were created at the same time as the prototype to test different geometries for bonding, and that will be explored in Section 5.3.

The other major geometry change of the structure was switching the side of the wing pivot that the driving force would act on. In the initial design, a class 3 lever was being used. The effort was being applied between the fulcrum and the load. This has a lower mechanical advantage when compared to a class 1 lever, which places the fulcrum between the effort and the load. This will decrease the force required to flap the wings, but also decreases the flapping angle for the same displacement [18]. The final kinematic sketch with its dimensions is shown in Figure 34.

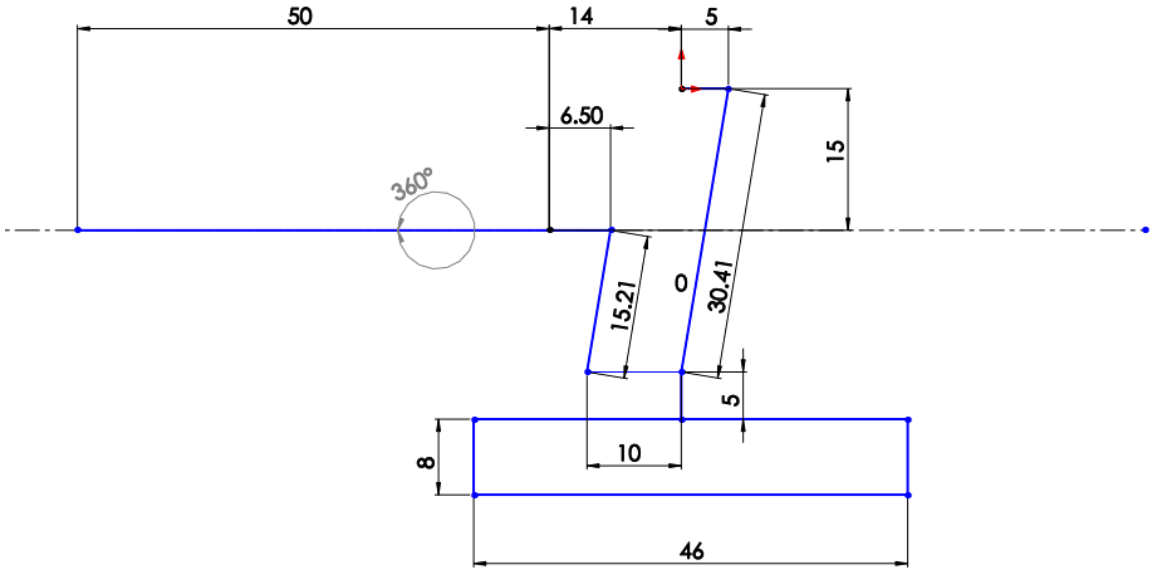


Figure 34: First Prototype Kinematic Sketch

### 3.4 Analysis of Design

This design features two parallel guiding mechanisms acting as springs in parallel on the slider, shown in Figure 35. The effective spring constant of the mechanism is thus double the spring constant of each parallel guiding mechanism. The final dimensions of the compliant mechanism are shown in Figure 36.

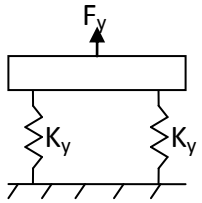


Figure 35: Spring Model of First Prototype

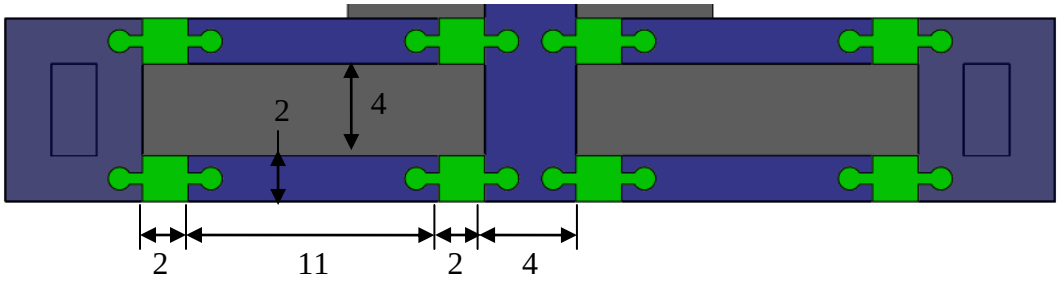


Figure 36: Dimensions of the Combined Parallel Guiding Mechanism

The stiffness of the mechanism given by the PRBM is 65.3 N/m. SolidWorks FEA does not offer the ability to simulate a single body with two different materials so a different approach was used for this iteration. The mechanism was simulated using ANSYS FEA software. A screen shot of the setup is shown in Figure 37.

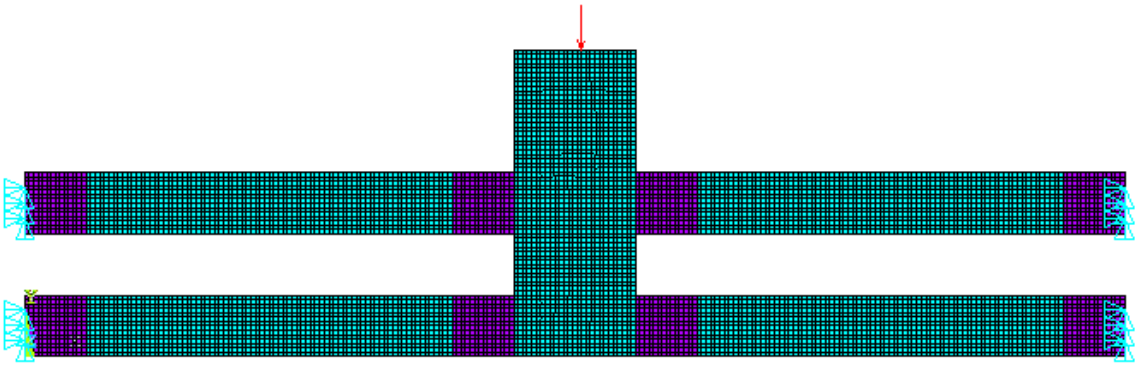

Figure 37: ANSYS Setup for Stiffness Simulation

The joints were modeled without the complex geometry and were approximated as squares. The elements were joined together using the glue function. The boundary conditions applied were the fixing of joints on their free ends. A force was applied in the vertical direction on the middle rigid body. The results of the analysis are shown in Figure 38. The comparison of the results to the PRBM is shown in Table 4. The PRBM again predicts a higher stiffness than the FEA model. Again, the assumption will be made that this is due to the large deflection of the mechanism.

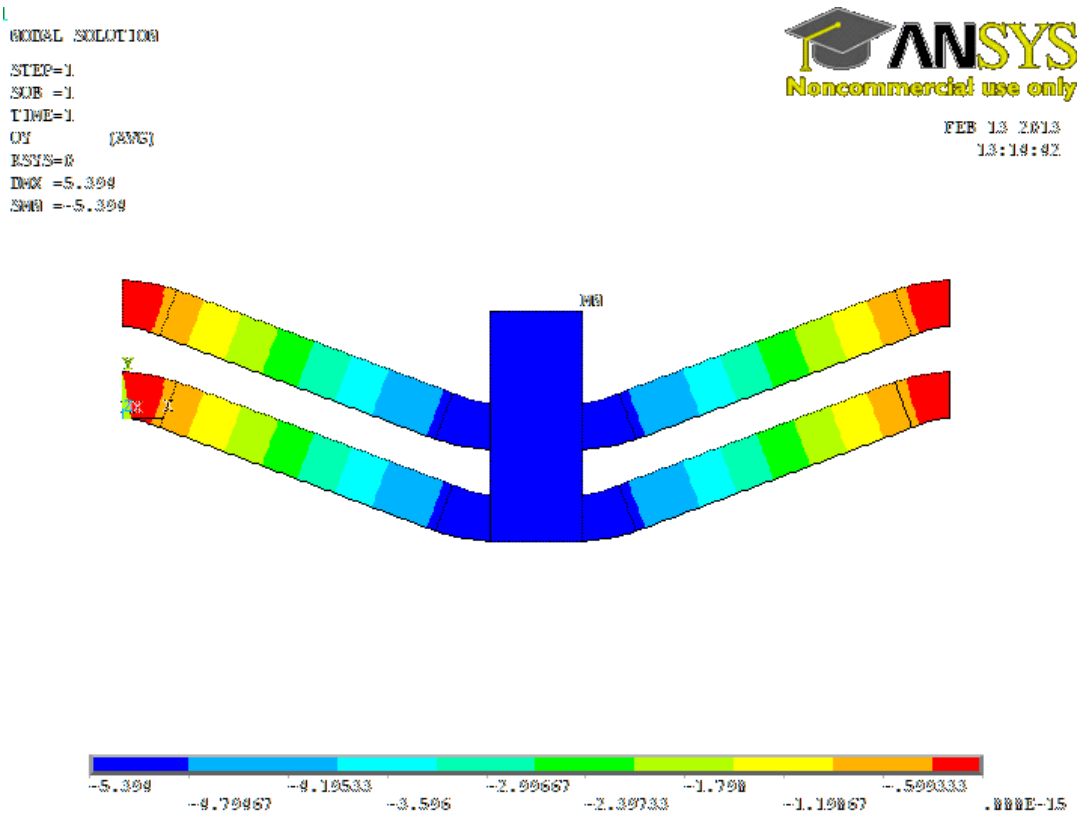


Figure 38: ANSYS Results for Prototype

Table 4: Stiffness of Prototype Mechanism

| Method | PRBM | FEA | % Difference |
|---|---|---|---|
| Stiffness, $K_m$ (N/m) | 65.2 | 27.8 | 57.4 % |

An Adams model was created to approximate the torque required and lift produced. The setup is shown in Figure 39. The results for lift and torque are shown in Figures 40 and 41, respectively.

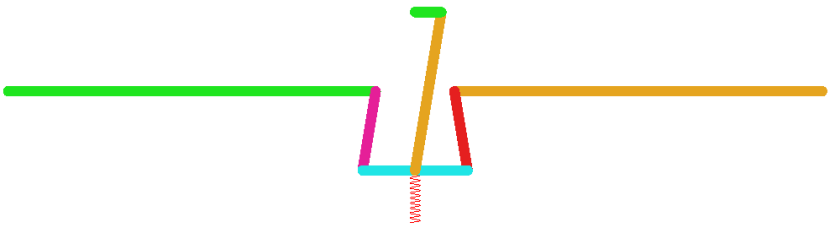

Figure 39: Adams Model of Prototype

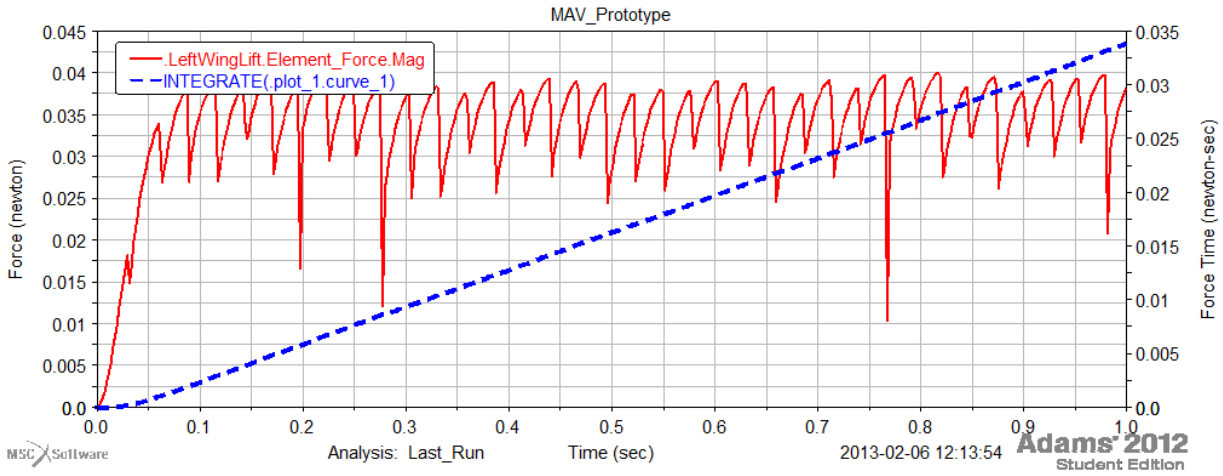


Figure 40: Theoretical Lift Produced by Prototype

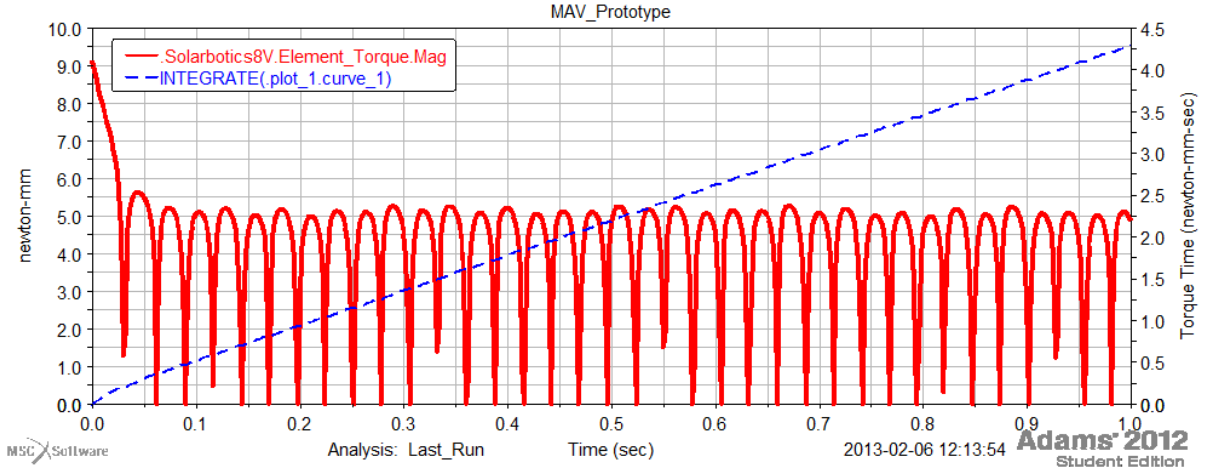


Figure 41: Theoretical Torque Required from Motor

The theoretical lift production has improved to the capability of lifting 7.1 grams. The torque is still within the capabilities to operate.

## 3.5 Other Components of Design

The final design is shown in Figure 42. There were a few components of the design that had not been fully developed in the initial design. These included the other small angle deflection joints throughout the structure, the pivot points for the crank-coupler interaction and the wings, and the design of the wings themselves.

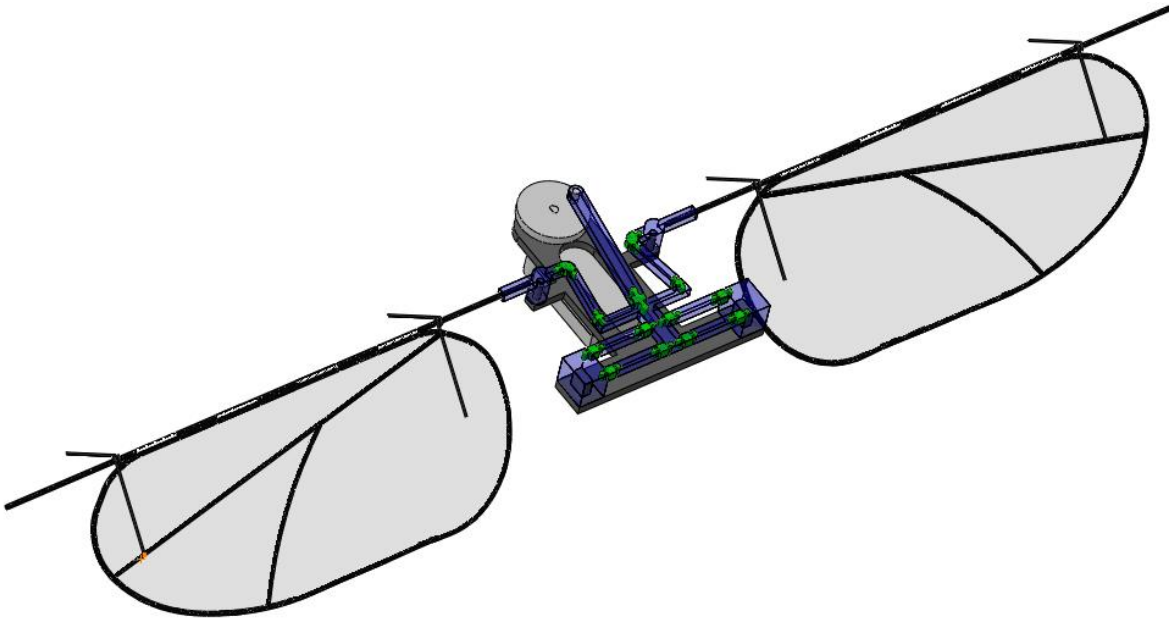

Figure 42: Final Design of MAV Prototype

The preliminary design called for joints to be embedded in the polypropylene structure. After choosing to use two materials in the design, it was decided to use joints similar to the ones seen in the compliant mechanism to allow the rest of the structure to flex. These joints are seen in green throughout the structure.

The pivot pins were initially going to be a raised boss of polypropylene. It was decided the strength of these would not be high enough to endure the shear on the pins. Precision doll pins were found that could be press fit into holes in the bottom layer. The top layer would have an oversized hole to allow for free rotation about the pin.

The motor no longer was to be embedded into the structure. It was determined that it would be just as secure to press fit the motor in place. This would save having to machine in a cutout for the motor to be placed in and protecting its electrical components.

To connect the wings to the structure, carbon fiber rods were embedded into the top layer. This would allow different wings to be created and attached to this rod. Different designs

would be tested to determine an optimum wing shape. The main focus of the design was on the mechanism and thus the wing design became a secondary aspect.

Ideally, active wing control would be implemented. Active wing control involves using a mechanism to control the angle of attack of the wing throughout the flapping motion. This would allow maximum lift to be produced. With the current design, wing control would be passive. It uses the change in the flapping direction and the drag created to allow the wing to switch its angle of attack from 45° to -45°. Stops will be created to control these positions. This decreases the average coefficient of lift produced, but is simpler to design and control.

The total weight of the structure is predicted to be 9.5 g. A break down the weight of the different components is shown in Table 5. As can be seen, the MAV still does not produce enough lift. The wings are currently estimated and it is not known what their actual weight will be. The structure now makes up the majority of the mass and will be the focus for decreasing the weight.

Table 5: Weight Distribution of MAV

| Part | Weight | % of Weight |
|---|---|---|
| SDM Structure | 4.3 g | 45.3% |
| Solarbotics GM15 Motor | 1.3 g | 13.7% |
| Wings | 1.7 g | 17.9% |
| Full River Batteries | 2.2 g | 23.1% |

# CHAPTER 4: SHAPE DEPOSITION MANUFACTURING PROCESS

## 4.1 Overview

The general shape deposition manufacturing process takes a minimum of three steps. The first step is to create the mold for the material. This is followed by pouring the material into the mold and allowing it to cure. Finally the part is extracted from the mold. This design will

use five steps. The first two steps will be repeated twice for the two separate materials. One can only pour one material at a time.

## 4.2 Create First Mold

The first material to be molded was the stiffer urethane plastic. The mold was machined out of a wax block using a Computer Numerical Control (CNC) machine. A model of the mold was created in SolidWorks and a G-code, which is used by the CNC, was created using CAMaster. The model of the mold is shown in Figure 43 and the machined wax block is shown in Figure 44. The top half of the wax block is dedicated to the sample links that were tested and discussed in Section 5.3. The bottom half is the parts for the MAV.

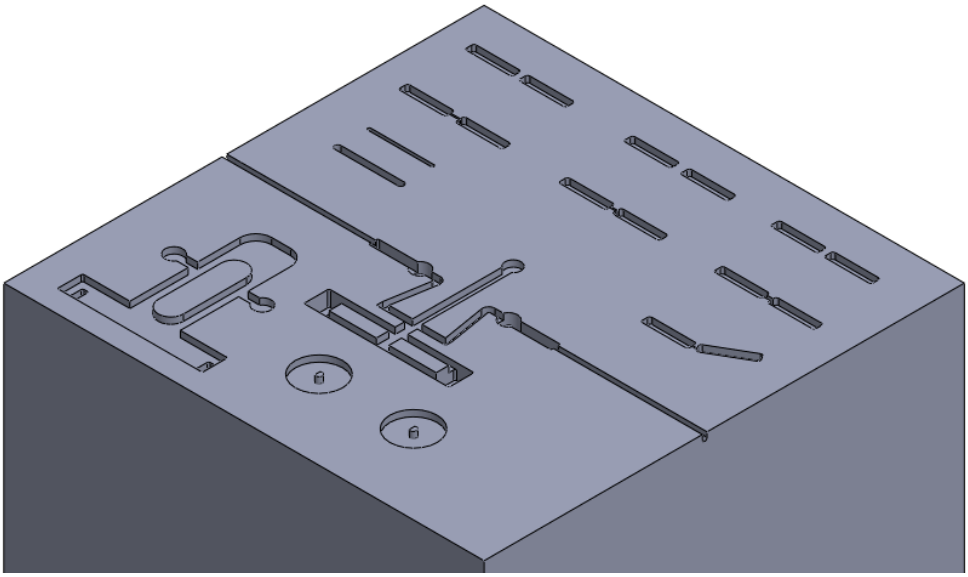

Figure 43: Model of Wax Block for Mold

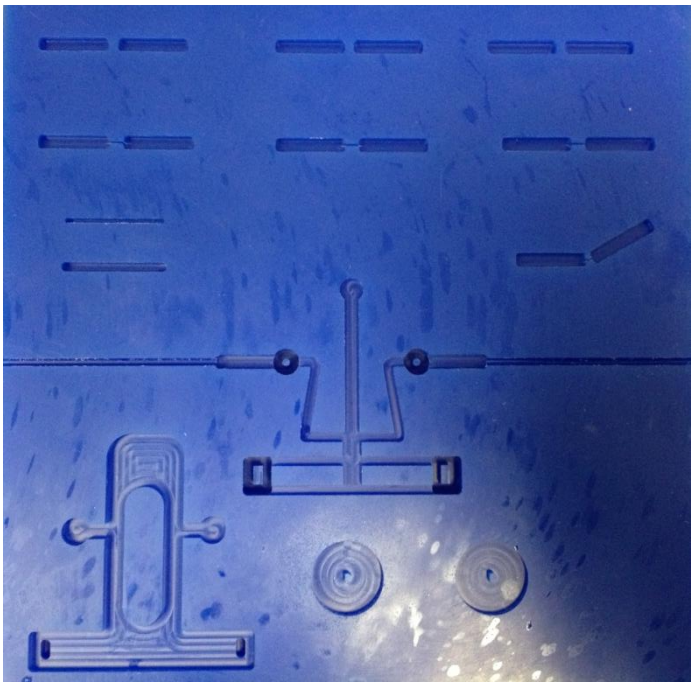

Figure 44: Mold Machined into Wax Block

### 4.3 Pour First Mold

The TASK© 9 was the first material poured. The material comes separated in two parts, A and B. The two parts were mixed at a ratio specified by the supplier and then put in a degassing chamber, shown in Figure 45. This was used to remove any possible bubbles that can formulate when mixing the two parts. If a bubble was in the mixture and it ended up in the mold, then that severely diminishes the quality of the structure. Prior to pouring the mold, any components that were to be imbedded in the material were placed in their respective location. In this design, carbon fiber rods were placed in the structure for the wings. Since a groove was created for the rod, and material was not desired for the length of the groove, clay was used to cover this area so that material did not get in. After the mixture was degassed, it was poured on top of the mold, as shown in Figure 46. Duct tape was placed around the edges of the wax block to keep the material from spilling over the edges. Hypodermic needles were used to remove any

bubbles that could be seen in the mold following the pour, as shown in Figure 47. The mold was then allowed to cure for the specified time.

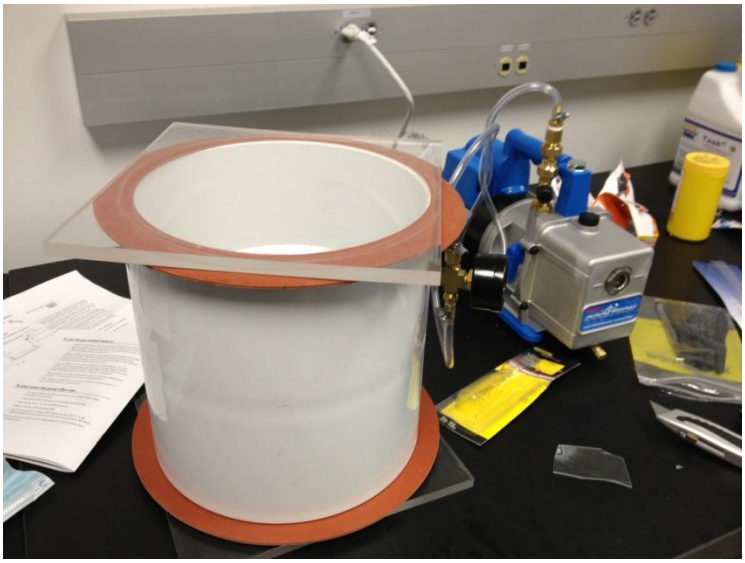

Figure 45: Degassing Chamber

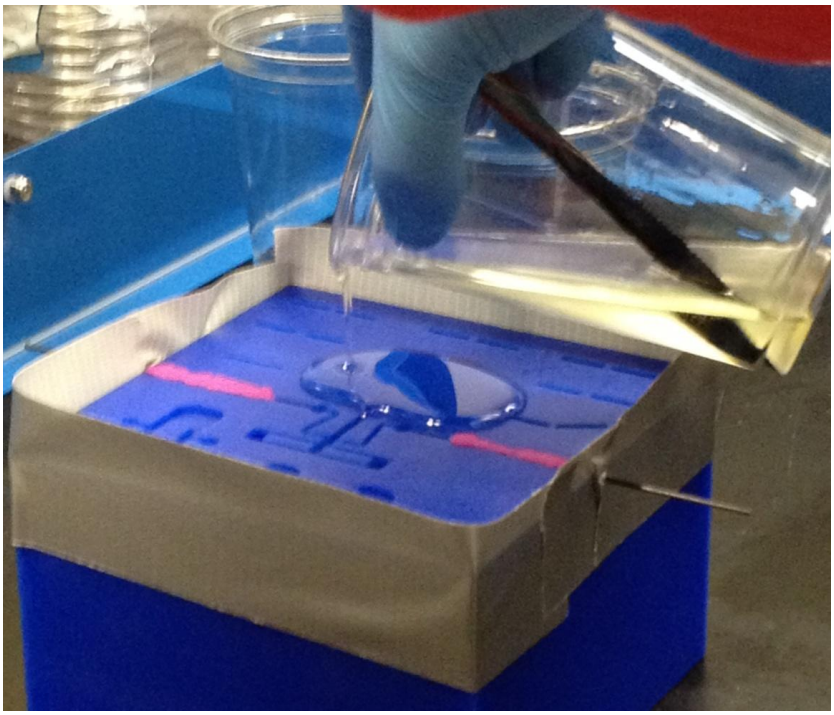

Figure 46: Pouring the First Mold

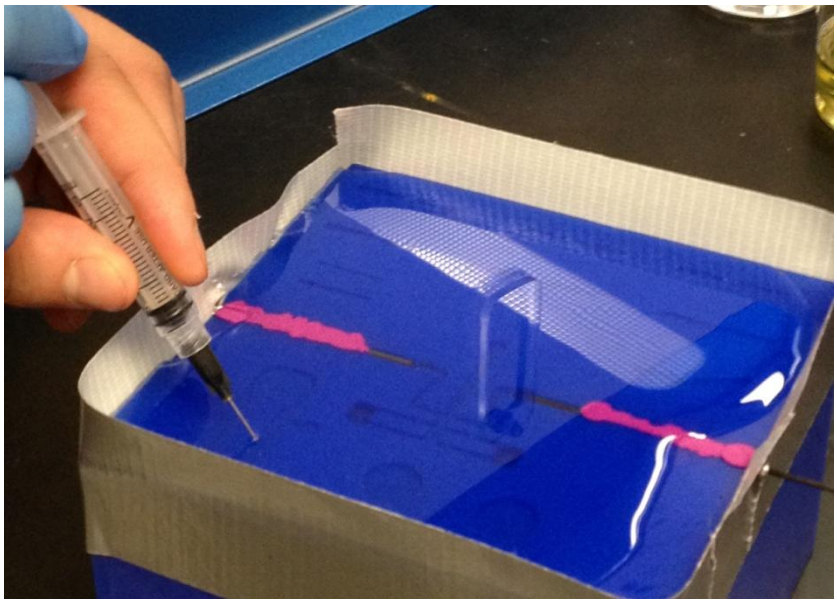

Figure 47: Extracting Bubbles using Hypodermic Needles

## 4.4 Create Second Mold

After the urethane plastic cured, the wax block needed to be planed back to its original surface to remove the excess material. A model for the mold of the parts that required the second material, VytaFlex© 60, was created, and is shown in Figure 48. Extraction paths were also cut into the wax block. These were cuts around the structure that would allow a pick tool to get underneath the part and allow for easier extraction. The actual block before pouring the mold is shown in Figure 49. Clay has been placed in the extraction paths to prepare for the pouring of the flexible material.

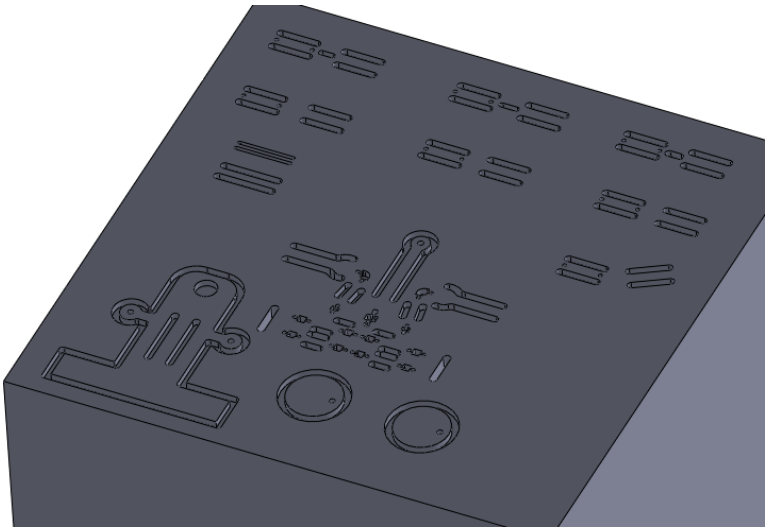

Figure 48: Model of Wax Block for Second Mold

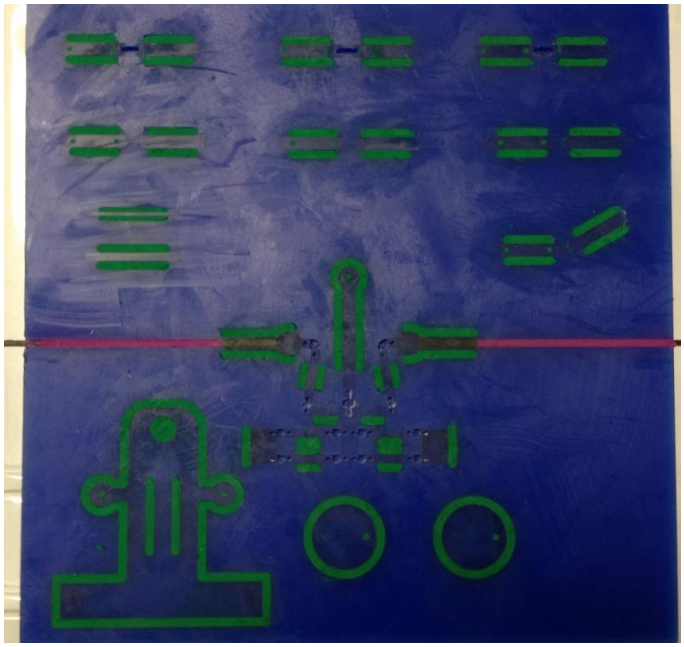

Figure 49: Wax Block before Pouring Second Mold

## 4.5 Pour Second Mold

The process for the second material was similar to the first in that there were two parts and the mixture was degassed. Following the pouring of the material however, a razor blade was used to smooth the material to the surface, as shown in Figure 50. This would make it so that the

surface would not need planed again. The material was then allowed to cure before moving on to extraction.

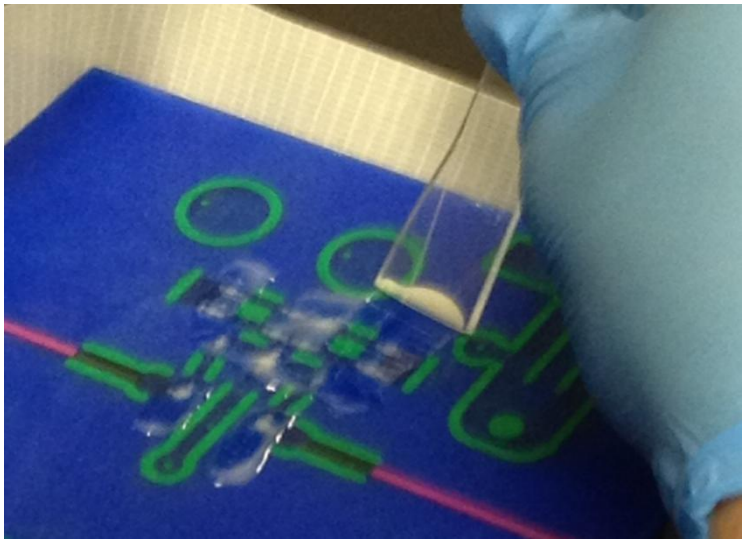

Figure 50: Using Razor Blade to Remove Excess Material before Curing

### 4.6 Extraction

The clay was first removed from the extraction paths. Then picks were used to pry the parts out of the mold. Care has to be taken as this is a slow and gentle process. If too much force is placed on one section, it may break the part.

## CHAPTER 5: FIRST PROTOTYPE FINAL ASSEMBLY AND RESULTS

### 5.1 Final Assembly

The parts that were extracted from the mold were almost completely to specification. The only fault that occurred was one of the wing arms broke off during extraction. This was most likely due to the design. The embedded carbon fiber rod ended right where the cross section of the material thinned out. This created a weak point in the structure and was susceptible to breaking during extraction.

The top and bottom layers snapped together as designed without a problem. The pins were pressed fit in the bottom layer and the top layer was able to rotate about them freely. The motor was also press fit into the bottom layer and the crank was press fit onto the D-shaft. While testing the mechanism by hand, it became apparent that the top layer was able to easily slip off the rotating pins because nothing was constraining it on them. It was decided to create a through hole on the top layer and to peen the end of the pin to constrain the top layer. This was a successful design improvement and did not disrupt the flapping motion. The final assembled prototype is shown in Figure 51.

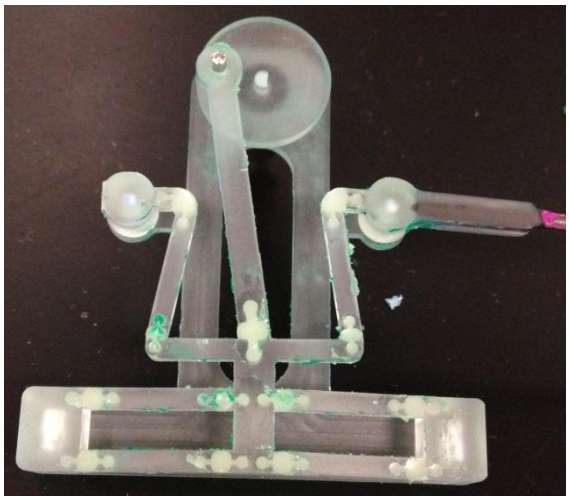

Figure 51: Final Assembled Prototype

## 5.2 Observations of Prototype

Upon testing the mechanism by hand, it felt noticeably stiffer than expected. The force required to displace the mechanism 5 mm was calculated to be less than 1 N during the design phase. When pulling on the mechanism with a spring scale, it was determined that it took at least 5 N to displace 5 mm. This means the motor would not be able to produce enough torque to displace the structure. The increased stiffness of the mechanism will be explored more in Section 5.4.

Other than the mechanism being too stiff, it performed as expected. It was capable of reaching the bounds established and the wings rotated as expected. The flexible links throughout the structure were stiff enough to hold their shape but flexible enough to allow the mechanism to perform.

When the mold for the stiff material was created, it was decided to pour the stiff material where the flexible material would need to be poured later to simplify the machining of the first mold. The CNC mill then cut into the stiff material to create the mold for the flexible material. After the parts were inspected following extraction, it was noticed that there was some stiff material left where the machining took place for the flexible material. This was not a large issue, but was noted for later designs.

The overall weight of the structure following assembly was determined to be 9.6 g. This compares to the expected weight of 9.5 g. The structure still does not contain the wings, so it will be heavier. The wings have not been created because the mechanism does not function properly and the wings would not flap. The excess weight is due to the wiring of the batteries. The estimated weight only took into account the batteries themselves. The batteries had to be wired in series, as well as wired to a switch and a motor.

### 5.3 Observations of Sample Links

During the fabrication of the MAV, some sample links were created on the same block. The goal was to study different geometries of links and to see how well the two materials bond together. The links were tested through both bending and tension to determine their respective elastic moduli and to attempt to make the flexible joint fail. With very simple geometry, a slot, the joints were able to stretch over 100% without separating from the rigid material. This showed that for the next prototype the joints can take on a much simpler geometry without worry

about slipping. When testing the material for the different moduli, it was noted that there was some difference between the manufacturer's specifications and the experimental results. The tensile modulus was given as 300 psi. The experimental results were that the tensile modulus was 100 psi and the bending modulus was 500 psi. The differences in the results were noted and will continue to be tested. It may be due to non-precise mixing ratios or different testing procedures.

### 5.4 Reason for Increased Stiffness

The assumptions that were made for the stiffness calculation were incorrect. The PRBM is only accurate for small deflections. Here the accuracy decreases significantly when stretching of the joints becomes involved. What wasn't taken into account when estimating the stiffness of the structure was the force it would take to stretch the joints the extra length. An illustration of the stretching of the joints is shown below in Figure 52. The force required to stretch the joints is found by using the stress strain relationship shown in Equation 12. The force required to displace the structure 5 mm vertically is 3.2 N. This gives a stiffness of 640 N/m, which is almost 10x the earlier predicted stiffness using solely the PRBM.

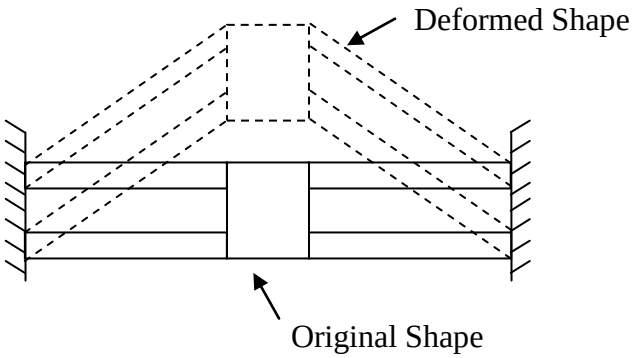


Figure 52: Original and Deformed Shape of Parallel Guiding Mechanism

$$\frac{F}{EA} = \frac{\Delta l}{L} \tag{12}$$

The ANSYS model was inaccurate as well. It is not known for sure what caused this, but it is suspected that using linear elastic material properties may have been at fault. When stretching rubber, the elastic modulus is not linear elastic. It behaves more like as shown in Figure 53 [19]. Using ANSYS will be avoided in future iterations until a more accurate model can be generated.

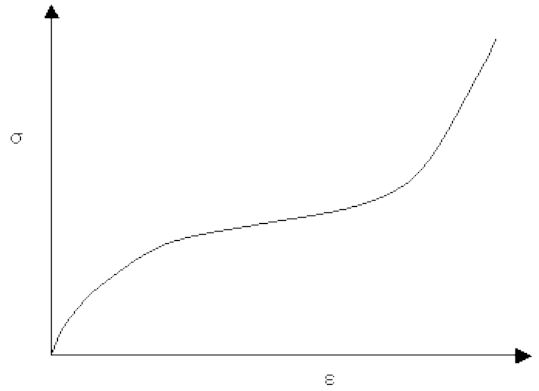


Figure 53: General Stress-Strain Curve of Rubber Materials

## 5.5 Conclusions of First Prototype

The results of the first prototype have provided guidance for redesigning the second prototype. First, it has been confirmed that SDM can be used to manufacture MAVs. The mechanism was able to flex as expected. The problem with the design, too high of stiffness, was due a calculation error, not fabrication. To fix this problem the idea used in the initial design, two layers of parallel guiding mechanisms, will be incorporated into the second prototype. This will solve the problem because it takes stretching out of the equation. When there is just one layer, the two ends are fixed and the joints must stretch. When there are two layers, the ends are able to move inward toward the center of the mechanism and the joints experience almost pure bending.

The testing of sample links showed that simple joint geometry may be used. The first prototype took significant machining time to complete the joints. With the joint geometry being slots, the machining time will be cut down significantly. The other thing that was noted from the sample links is the modulus specified by the supplier may vary based on how well the mixing ratios are followed. Further testing will be completed to see the variance of the modulus during different trials.

There are two areas that will be improved in the second design. The wing on the first prototype broke off during extraction. To decrease the chances of this occurring again, the carbon fiber rod will be moved away from the area where the cross section decreases in size. This cross section will also be slightly increased in size. The second area is accounting for the peening of the pins. The top layer will have through holes, as modified in the first prototype, which will constrain the top layer to stay connected with the bottom layer.

# CHAPTER 6: SECOND PROTOTYPE DESIGN

## 6.1 Design Changes to Compliant Mechanism

As mentioned previously, a simpler joint geometry would be used in the second prototype. Also a second layer will be added to the parallel guiding mechanism which will decrease the stiffness, as shown in Figure 54. This moves the fixed point of the mechanism from the two ends to the inside, which effectively allows the ends to translate inwards. This removes stretching from the calculation. The redesigned mechanism is shown in Figure 55. The only other change was for the embedded carbon fiber rods. The thickness around the carbon fiber rod was increased and the rod was moved away from where the cross section decreased.

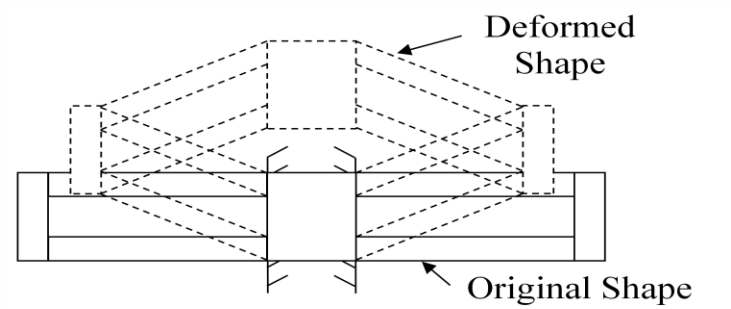


Figure 54: Original and Deformed Shape of Second Prototype

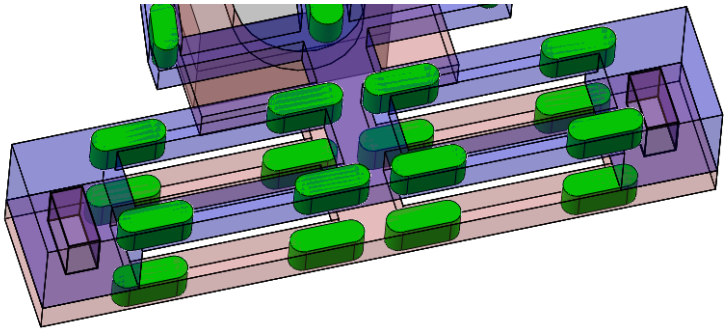

Figure 55: Compliant Mechanism of Second Prototype

## 6.2 SDM Process

The same SDM process was followed as outlined in Chapter 4. The models of the molds for the stiff and flexible materials are shown in Figures 56 and 57, respectively. The wax block is shown following the pouring of the second mold in Figure 58.

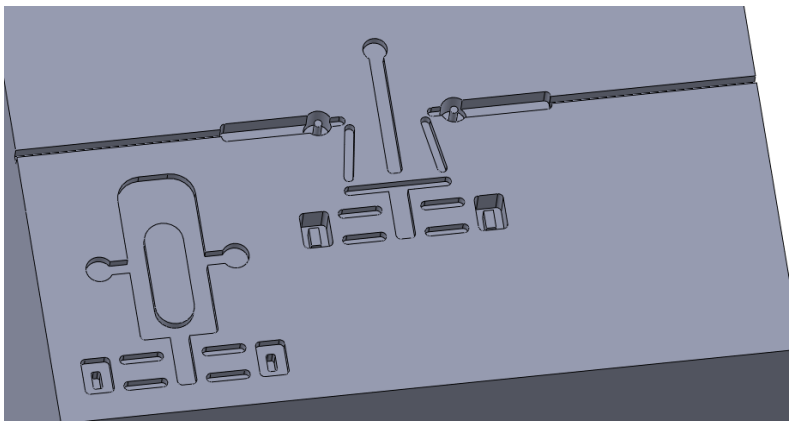

Figure 56: Model of First Mold for Second Prototype

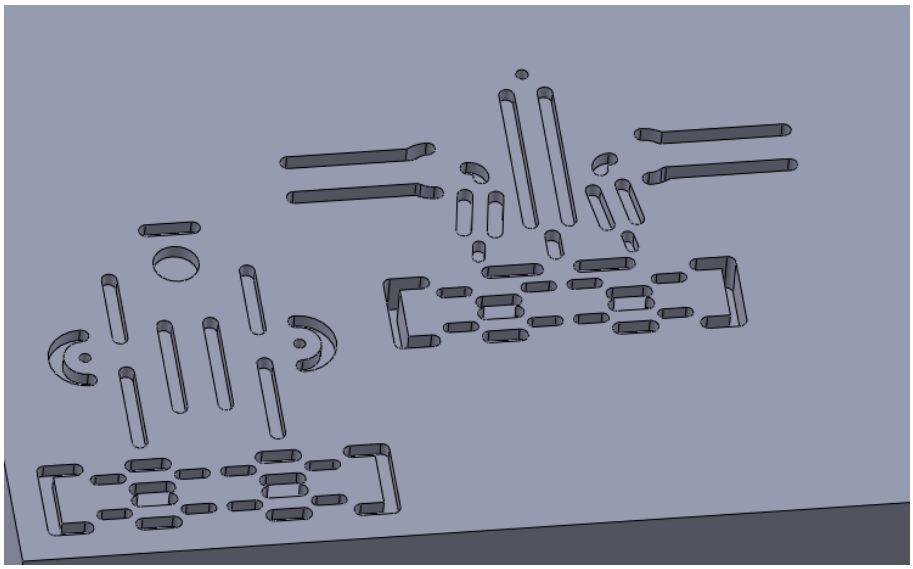

Figure 57: Model of Second Mold for Second Prototype

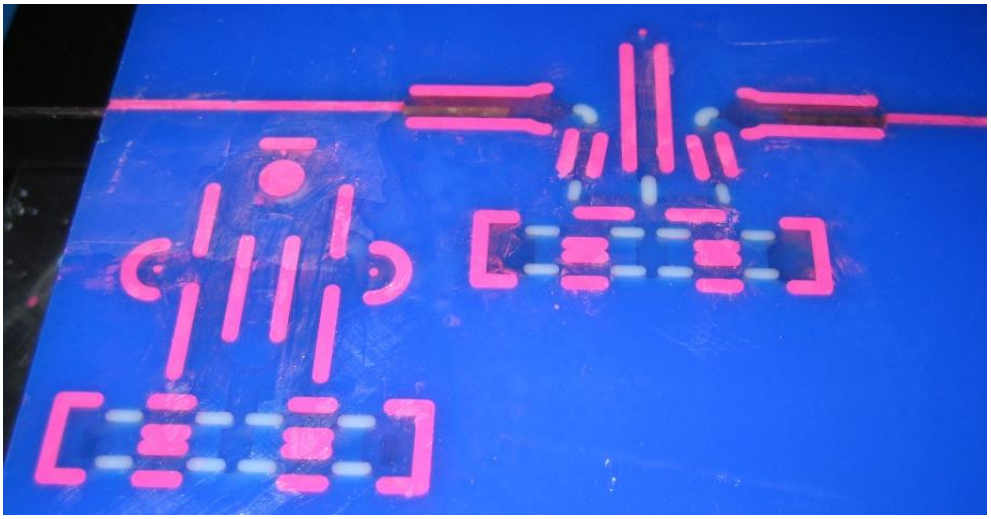

Figure 58: Wax Block for the Second Prototype

## 6.3 Second Prototype Results

The second prototype again performed kinematically as expected. The SDM process was shown to produce a MAV that has the ability to function. There was only one error during the SDM process. Clay accidently got into the mold after the rigid material had cured and machined, but before the flexible material had been poured. The oil or residue left over from the clay provided a less than ideal bonding surface between the two materials and the joint between the

wing activator and the wing became disconnected. The bond was patched using super glue, but will not have the same life expectancy as a natural bond between the two materials. To prevent this from happening again, more caution must be taken to avoid clay getting into the mold before the material is poured.

The mechanism was first tested using a spring scale to measure the force required to displace it 5 mm, the length of the crank. The stiffness was found to be about three times the expected stiffness, .8 N compared to .25 N. The reasons are not completely known at this point but one idea is that the other flexible joints in the MAV are not modeled in the PRBM and therefore could be a source of extra stiffness.

With the extra stiffness, the motor should still be able to produce enough torque to make the MAV flap without wings. When connecting the motor to a power source, the MAV still did not produce a flapping motion. Tests were completed to determine how much torque the motor could produce. It was found the motor was producing about ten times less torque than given in the specification. Our lab was able to determine the motor used for the MAV had been damaged at some point. When spare motors were tested, they produced a stall torque that more closely followed the specification given by the manufacturer. These motors had not yet been connected to the MAV however as they have a different shaft geometry, and are not compatible with the current crank. The spare motors will be modified to be compatible with the current design and to become closer to creating a functional prototype that may be tested. Once the prototype is functional, testing will be able to be completed to determine the usefulness of this design.

# CHAPTER 7: CONCLUSION

The purpose of this work was to design and fabricate a light weight flapping wing MAV using techniques that had not previously been explored.

## 7.1 Contributions

MAVs have been increasingly studied recently to develop a tool for completing reconnaissance missions, chemical and biological detection, and surveillance in unstable areas. This work studied two different techniques that have not previously been explored when designing MAVs. The more successful technique was using shape deposition manufacturing to fabricate a MAV. Two prototypes were built using SDM and the usefulness of this process was revealed. Both prototypes were relatively cheap to manufacture and functioned properly.

The second technique that was studied was using a compliant mechanism to replace the slider and reduce losses. The positives of using the compliant mechanism were the reduction in part count and ease of assembly. The mechanism eliminates the friction that would be seen from a slider and stores energy instead of it being dissipated. However, the compliant mechanism takes up a significant amount of space and makes up a large percentage of the mass. It may be more beneficial to embed a linear bearing to reduce the friction at the slider joint than to replace it with the mechanism. It also adds a large amount of complexity to the analysis. The technique will be further explored and optimized.

This paper has outlined the design approach used while creating multiple designs and prototypes. One could use this approach to continue to iterate the design and improve upon it. Others could also learn from this approach to improve on their design abilities.

## 7.2 Additional Applications

This paper has shown how SDM and compliant mechanisms couple well together. These techniques can be and have been combined in many other areas besides MAVs. The design process outlined in this paper can be applied to all of these different areas.

## 7.3 Future Work

The current design of the MAV is far from optimal. There are many areas that can be improved upon. The wings have not been fully developed. Once a functional prototype is created, different wing shapes and sizes can be attached to the MAV and studied to find an optimal design. As mentioned earlier, it should be studied if using a linear bearing for the slider is more beneficial than using a compliant mechanism. The materials being used also need to be studied more. Tests need to be performed to determine actual material properties and what type of joint geometry is required for the different material interactions. Implementation of active wing control would be optimal and will generate significantly more lift than using passive wing control.

## 7.4 Summary

A flapping wing MAV was designed, analyzed, and fabricated. Two previously unstudied techniques were used when designing and fabricating the MAV. These techniques were using a compliant mechanism to replace the slider in a crank-slider mechanism and using SDM to fabricate the prototype. SDM was successfully used to create two different prototypes. The first prototype did not perform as expected. It was shown that there was an error in the stiffness calculation and this was compensated for in the second prototype. The second prototype is currently being studied to see if using compliant mechanisms is beneficial to the design. This study will be beneficial in exploring new techniques in the MAV design process.

# BIBLIOGRAPHY


[1] J. M. McMichael and M. S. Francis, "Micro Air Vehicles - Toward a New Dimension in Flight," 7 August 1997. [Online]. Available: http://www.fas.org/irp/program/collect/docs/mav_auvsi.htm.

[2] L. Petricca, P. Ohlckers and C. Grinde, "Micro- and Nano-Air Vehicles: State of the Art," *International Journal of Aerospace Engineering,* pp. 1-17, 2011.

[3] J. Grasmeyer and M. Keennon, "Development of the Black Widow Micro Air Vehicle," in *39th AIAA Aerospace Sciences Meeting and Exhibit*, 2001.

[4] W. Thielicke, "Shrediquette - A Multirotor MAV," 9 May 2010. [Online]. Available: http://shrediquette.blogspot.com/2010_05_01_archive.html. [Accessed 1 March 2013].

[5] M. Keennon, K. Klingebiel, H. Won and A. Andriukov, "Development of the Nano Hummingbird: A Tailless Flapping Wing Micro Air Vehicle," in *50th AIAA Aerospace Sciences Meeting including the New Horizons Forum and Aerospace Exposition*, 2012.

[6] Z. Khan, K. Steelman and S. Agrawal, "Development of Insect Thorax Based Flapping Mechanism," *IEEE International Conference on Robotics and Automation,* pp. 3651-3656, 2009.

[7] L. Howell, Compliant Mechanisms, New York: John Wiley & Sons, Inc., 2001.

[8] "The Shape Deposition Manufacturing Process," Carnegie Mellon Univeristy, [Online]. Available: http://www.cs.cmu.edu/~sdm/methodolgy.htm. [Accessed 1 March 2013].

[9] R. Merz, F. Prinz, K. Ramaswami, M. Terk and L. Weiss, "Shape Deposition Manufacturing," Engineering Design Research Center, Carnegie Mellon University, 1994.

[10] C. Galinski and R. Zbikowski, "Some Problems of Micro Air Vehicles Development," *Bulletin of the Polish Academy of Sciences: Technical Sciences,* vol. 55, no. 1, pp. 91-98, 2007.

[11] C. Bolsman, "Flapping Wing Actuation Using Resonant Compliant Mechanisms: An Insect Inspired Design," Development Labratories, Eindhoven, 2010.

[12] "GM15 Motor," Solarbotics, 2011. [Online]. Available: https://solarbotics.com/product/gm15/. [Accessed 11 December 2012].

[13] D. Pines and F. Bohorquez, "Challenges Facing Future Micro-Air-Vehicle Development," *Journal of Aircraft,* vol. 43, no. 2, pp. 290-305, 2006.

[14] J. McPherson, "Complete Guide to Lithium Polymer Batteries," RC Groups, 20 September 2003. [Online]. Available: http://www.rcgroups.com/forums/showthread.php?t=209187. [Accessed 7 March 2013].

[15] "Full River 30 mAh Cell," BSD Micro RC, [Online]. Available: http://bsdmicrorc.com/index.php?productID=530. [Accessed 7 March 2013].

[16] S. Nogar, J. McNamara, A. Serrani, M. Oppenheimer and D. Doman, "Development of a Fundamental Model for Flapping Wing MAVs and Preliminary Validation," in *AIAA Atmospheric Flight Mechanics Conference*, Minneapolis, 2012.

[17] "Smooth-On Home Page," Smooth-On, Inc., [Online]. Available: http://www.smooth-on.com/. [Accessed 7 March 2013].

[18] "Levers," The Engineering Toolbox, [Online]. Available: http://www.engineeringtoolbox.com/levers-d_1304.html. [Accessed 1 March 2013].

[19] "S-Shaped Curves," University of Cambridge, [Online]. Available: http://www.doitpoms.ac.uk/tlplib/bioelasticity/s-shaped-curves.php. [Accessed 1 March 2013].